Stray Light Analysis of a Mobile Phone Camera

Jordan Jur
College of Optical Sciences, University of Arizona, Tucson, AZ 85721
Master's Project spring 2016

ABSTRACT

Stray light, defined as unwanted light or energy [1], is an unintended consequence which degrades the designed functional performance of an optical system. For optical imaging systems, the designed functional performance is quantified by the diffraction based image quality metric of MTF. Traditional optical design software's, like ZEMAX, only correct for aberrations influenced by the first order system parameters, such as, f-number and field of view [2].   However, optical analysis software's, like FRED, consider the effects which coatings and mechanical structure have on image quality. These parameters are known as stray light sources and are divided into specular and scatter components. Here we demonstrate that well-established mitigation strategies, specific to specular and scatter mechanisms, can be utilized to minimize stray light. The results indicate that specular contributions can be mitigated with improved AR coatings, the scatter contributions can be mitigated with cleanliness control and structure material selection while a cylindrical lens barrel design over a conical one improves both contributors.

I. INTRODUCTION

Due to the evolution of the mobile phone market over the past decade consumers have come to expect more from the designers and manufacturers of their mobile devices. When cameras were first introduced to the mobile phone platform expectations were low due to the unfamiliarity of such a feature on a mobile device. As cameras became a prevalent feature on the mobile phone, consumer expectations rose which promoted a new realm of competition within the market. As the competition increased, so did the complexity of the performance related challenges for the design and manufacturability of the mobile phone camera. Fast forward to present day and we see that one of these major performance related challenges is stray light mitigation; the topic of this project1[1].

Stray light is unwanted scattered or specular light or energy at the detector of an optical system, which is not intended in the optical design. In essence, stray light will degrade the MTF and resolution of the mobile phone camera and must be minimized. The sources and mechanisms of stray light have been studied since the 1950's and mitigation strategies have been well developed for some of the less complex entities. This project will examine and measure the specular and scatter contributors to stray light within a FRED optical model and employ some of the common mitigation methods to minimize stray light. An example of one type of specular stray light contributor, known as a ghost image, can be viewed in figure 1. This picture was taken with an iPhone 6 camera.

---

[1]Given the vast array of stray light sources, the mitigation techniques discussed in the following sections will only consider nominal design values and neglect perturbations inherent to the manufacturing process. For an accurate stray light analysis of a manufactured optical system, these manufacturing perturbations should be considered. See "Molded Optics: Design and manufacture by Michael Schaub for more information.

Figure 1. Stray Light Ghost Images in iPhone6 Camera

II. STRAY LIGHT FUNDAMENTALS

In order to properly and effectively execute a stray light design, the sources and sensitivities of stray light must be well understood. This section will introduce the main sources of stray light common to imaging systems. In addition, the sensitivity to which the first order properties, geometry and materials of the iPhone 6 camera impact the stray light performance will be explored. Any environmental effects on the stray light performance will be ignored for this analysis.

Stray light behaves in sequential and non-sequential manners which follows the behavior of light as observed in nature. As a result, different modeling methods will need to be executed in order to measure the different contributions. A list of stray light sources common to imaging systems [3], divided into specular and scatter categories, are listed in table 1. Note that only the stray light mechanisms with a medium or high sensitivity will be considered for this project.

Mechanism Type	Mechanism	Modeling Method	Sensitivity
SPECULAR	Surface Reflections	Non-sequential Raytracing	Medium
	Detector Reflections	Non-sequential Raytracing	Medium
	Structure Reflections	Non-sequential Raytracing	Medium
SCATTER	Surface Micro-roughness	BSDF w/ First-Order N.S. Raytracing	Medium
	Structure Scatter	BSDF w/ First-Order N.S. Raytracing	Medium
	Particle Contamination	BSDF w/ First-Order N.S. Raytracing	High
	Material Bulk Scatter	BSDF w/ First-Order N.S. Raytracing	Low
	Stress Birefringence	BSDF w/ First-Order N.S. Raytracing	Low
	Fluorescence	BSDF w/ First-Order N.S. Raytracing	Low

Table 1. Stray Light Contributors

Understanding the specific variables which impact the magnitude of the specular and scatter stray light mechanisms will aid the mitigation strategy.

SPECULAR MECHANISM (GHOST PATHS)

Unlike the random nature of scattered rays, ghost rays are deterministic according to the law of reflection, law of refraction, and the grating equation. Due to their deterministic nature, anything which affects these laws is a considered as a variable which impacts the mitigation of the specular stray light contributions. Note that there are no diffractive optics used in this optical system therefore variables which impact the grating equation will not be explored.

It is common practice to coat the optics with an AR coating to minimize reflections within an optical system. Less surface reflection means that more light will be either absorbed or transmitted by the optic. The absorption of VIS light by plastic optics is very low therefore it can be inferred that less reflection generally implies more light is transmitted. By changing the transmission of a coated surface the specular stray light mechanisms can be controlled. Bare uncoated surfaces will have a Fresnel reflection and transmission components of 4% and 96%, respectively[2]. Plastic optics generally have poor performing coatings compared to glass optics but can still achieve AR coatings of 98% [4], [5].

In addition to altering the surface coating properties, optic edges may be baffled by some means. Plastic optics are commonly designed with flanges on their edges which act as mounting interfaces to opto-mechanic barrels [6]. These flanges not only aid in the mounting of the optic but also serve to reduce the number of sneak paths within the optical system. A baffle may block a direct line of sight from the universe to the detector, as shown in figure 2.
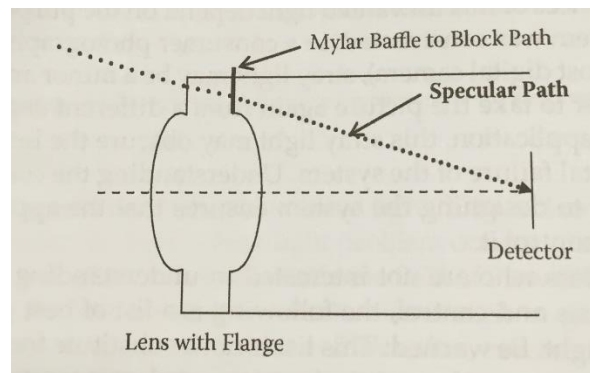

Figure 2. Opto-Mechanic Baffle

Lastly, the power (sag) of an optic surface should be minimized as to prevent a ray from being totally internally reflected. Once a ray TIRs off on surface it has the potential to TIR off another. In the case of plastic molded optics, the flange area provides a secluded set of surfaces which may contribute to TIR events and increase the specular stray light contributions. This mitigation technique is common practice for aberration control of the lens design and is known as lens bending or lens splitting [7]. In summary, specular stray light mechanisms can be controlled by altering the coating properties, adding baffles, and/or altering the optical design to minimize the power of a surface and the potential for a TIR event.

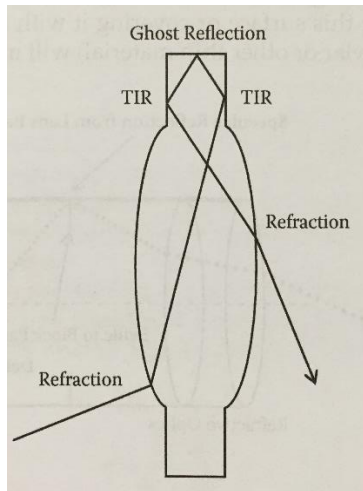[2] Assuming optic index of refraction is 1.5.

Figure 3. TIR Event

SCATTER MECHANISMS

Due to the nondeterministic nature of scatter light the analysis is a bit more complex. On the macroscopic scale, scattered light is light which cannot be described by the law of reflection, law of refraction, or the grating equation. The figure below illustrates scatter from a flat surface [8]. Note that the largest ray represents the specular reflection component whereas the smaller rays represent the scattered components.
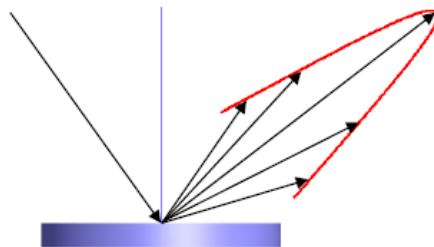

Figure 4. Scatter

The magnitude, distribution and direction of scattered light by a given surface is described by the bidirectional scatter distribution function (BSDF). In radiometric terms, the BSDF can be thought of as the ratio of the outgoing radiance to the incident irradiance. Therefore, BSDF has units of inverse steradians.

$$BSDF(\theta_i, \phi_i, \theta_s, \phi_s) = \frac{dL(\theta_i, \phi_i, \theta_s, \phi_s)}{dE(\theta_i, \varphi_i)} \tag{1}$$

where θ_i and ϕ_i are the angles of incidence and θ_s and ϕ_s are the angles of scatter in the three dimensional space described in Cartesian coordinates.   When the BSDF is integrated over 2π steradians the contribution of the scattered light can be quantified; this is known as the total integrated scatter or TIS. BSDF impacts the TIS of a surface which has a dependence on the surface roughness, wavelength,

and index of refraction of that specific surface. A more detailed, quantitative description of TIS and its impact on BSDF will be discussed in detail in section VI. A summary of the stray light mechanisms and their variables are listed in table 2 [3].

Category	Mechanism	Variables/Mitigation Strategy
SPECULAR	Surface Reflections	Optical Design, AR Coatings, and/or Baffles
	Detector Reflections	Optical Design, AR Coatings, and/or Baffles
	Structure Reflections	Optical Design, AR Coatings, and/or Baffles
SCATTER	Surface Micro-roughness	Material, Optical Polish Selection and/or Edge Blackening
	Particle Contamination	Cleanliness Control
	Structure Scatter	Optical and/or Baffle Design
	Material Bulk Scatter	Material Selection and/or Processing
	Stress Birefringence	Material Selection and/or Mounting Features
	Fluorescence	Materials Selection and Processing

Table 2. Summary of Stray Light Variables/Mitigation Strategy

Now that the variables which impact the specular and scattered stray light contributions are understood these concepts can be applied to a particular camera system. As a rule of thumb pointed out by Pfisterer, the following process should be executed when performing a stray light analysis [9].

Step	Task
1	Construct Optical Model
2	Construct Mechanical Model
3	Determine Critical Objects
4	Determine Illuminated Objects
5	Determine Common Objects
6	Construct Coatings and Scatter Models
7	Setup Importance Sampling
8	Perform Stray Light Analysis

Table 3. Stray Light Mitigation Process

III. OPTICAL MODEL

The optical model analyzed for this report is the iPhone 6 camera. The lens prescription was uploaded to ZEMAX based on the information provided in the patent literature [10]. It is common practice to not provide the exact lens prescription in the patent therefore a preliminary analysis of the optical system must be performed to ensure that decent performance is achievable from the prescription provided. The analysis will show that the information provided in the patent literature demonstrates decent performance and no optimization of the design is necessary.

The iPhone 6 camera consists of eight elements, including the aperture stop and detector, for a total of 15 surfaces. The first order parameters of the system are listed in table 4 and the optical layout can be viewed in figure 5.

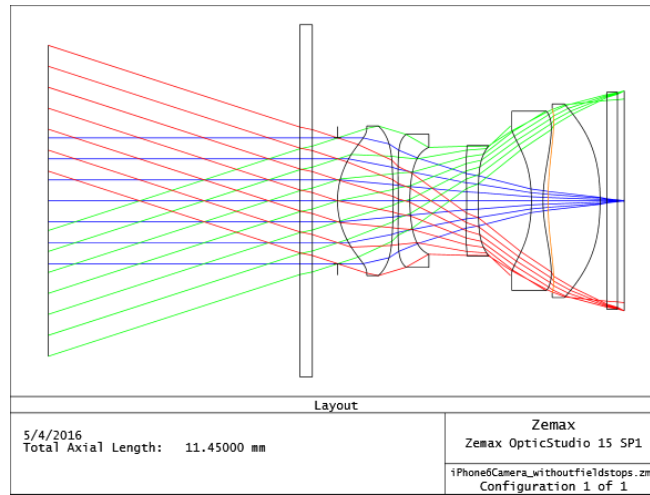| Parameter	Value
Focal Length (mm)	6.325
Diameter of EP (mm)	2.87
f/#	2.2
FFOV (°)	±18
No. Elements	8
Wavelengths	VIS Spec

Table 4. First Order Parameters

Figure 5. Optical Layout

The five lens are all 14th order aspheric surfaces (any surface which is not spherical) which is described by the polynomial deformation of a conic in equation 2.

$$z(r) = \frac{r^2/R}{1 + \sqrt{1 - (K+1)(r/R)^2}} + Ar^4 + Br^6 + Cr^8 + Dr^{10} + Er^{12} + Fr^{14} \tag{2}$$

where r is the radius of curvature of the surface, R is the half diameter of the surface, K is the conic constant of the surface, and A thru F are the aspheric coefficients. The exact values of these terms can be view in the optical prescription provided in figure 6.

Figure 6. Optical Prescription

LENS FUNCTIONS

Each lens in the camera is made from a specific material which has a funcion to control a certain aberration. The materials used in this optical system are list in table 5.

Element	Material	Brand Name	Refractive Index, n_d
Outer Window	Crystal	Sapphire	1.7715
Lens 1	COC	TOPAS® 5013	1.5333
Lens 2	PSU	Udel® P-1700	1.634
Lens 3	PSU	Udel® P-1700	1.634
Lens 4	COC	TOPAS® 5013	1.5333
Lens 5	PSU	Udel® P-1700	1.634
IR Filter	Glass	N-BK7	1.5168
Detector	Aluminum	iSight	-
Structure		PBT	-

Table 5. Camera Materials [11]

The outer window is the first element in this optical system and has a function to protect the lenes from the outside environment. It is made of sapphire which is a very hard material that will provide maximum resistance to scratches and other possible abrasions. The next element, the first lens, is located at the aperture stop, specifically, surface 1 of the first lens. Since this surface is located at the aperture stop it will only contribute to spehrical aberration [12]. In addition, this surface is the most powerful and as a results contributes the most spherical aberration to the system. Lenses 2 and 3 are meniscus lenses which correct for spherical aberration. They are also made of a flint plastic which can be used to correct for chromatic change in focus (LCA) and magnification (TCA) caused by the crown plastic of lens 1. Lens 4 surface 1 and lens 5 surface 2 are designed such that their radii of curvature for the speherical component lie nearly coincident with the aperture stop. This is significant because the chief ray goes through the center of curvature of these two surfaces and they will not contribute to any odd aberration which has a dependance on the chief ray height [13].
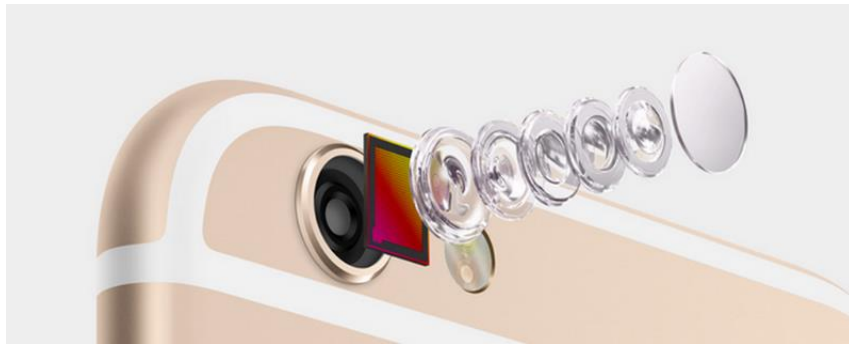

Figure 7. Exploded View

In addition, the higher order aspheric terms of lenses 4 and 5 serve to correct for astigmatism by means of flattening the field [7] and to limit the chief ray angle of incidence on the detector [14]. Controlling the chief ray angle of incidence allows for the control of the illumination of the image and will segway into the more detailed analysis section.

ANALYSIS

As is expected from any patent literature, the optical prescription provided is not ideal and will need to be analyzed. The relative illumination, known as irrandiance in radiometric terms, varies quartically with the chief ray angle of incidence, according to equation 3.

$$E = L\frac{A}{d^2}\cos^4(\theta)$$

(3)

where L is the radiance of an extended source, A is the area of the source, d is the distance from the detector to the extended source and θ is the angle of incidence of the chief ray on the detetor. Note that the quotient is the solid angle of detector subtends from the point of view of the extended object. Generally speaking, it is good practice to limit chief ray angle of incidence such that the relative illumination difference from the center of the optical axis to the edge of the image falls within the gain bandwidth of the detector. By doing so the detector can adequately compensate for the relative difference in illumination. The angle of incidence can be approximated using first order parameters, as shown in equation 4.

$$\theta = \arctan(h'/f)$$

(4)

where h' is the image height, found in figure 5, and f is the focal length of the optical system found in table 4. Equation 4 calculates the chief ray angle of incidence to be 17.14° which yields a theoretical relative illumination of 0.834. Using the "Relative Illumination" analysis function in ZEMAX, shown in figure 10, it is demonstrated that the relative illumination for this optical system is actually 0.521 (roughly 1.6X worse) partially becaue there is some vignetting through the system.

Figure 8. Image Simulation

Ignoring the vignetting affects of the pupil mismatch seen at the edge of the picture, the effect of the relative illumination can be observed in ZEMAX using the "Extended Scene Analysis" tool. Note that the on-axis, center portion of the image remains the same in both images and the image quality degrades as the image moves radially outward.

In addition to the relative illumination, there are other metrics of the optical design which were not ideal. Figures 9 thru 12 show many metrics commonly used to interpret the image quality. According to equation 5, the diffraction limited performance of the camera should yield a spot diameter of 2.95µm at λ=0.55µm. Note that this is the radius of the beam which contains 83.8% of the beam energy.

$$D = 2.44\lambda f/\#$$ (5)

For the prescription used for this analysis, the spot diameter which contains 83.8% of the beam is 3.058µm (Figure 12); roughly 1.036X worse. Ignoring the performance differences from the ideal diffraction limited case, the optical model still achieves adequate performance so that a stray light analysis can be performed.
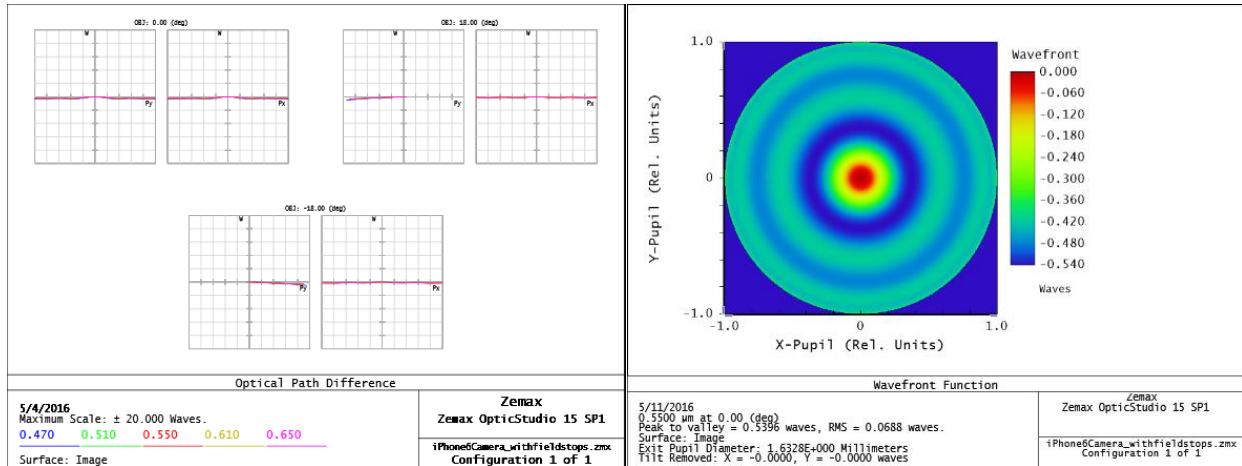

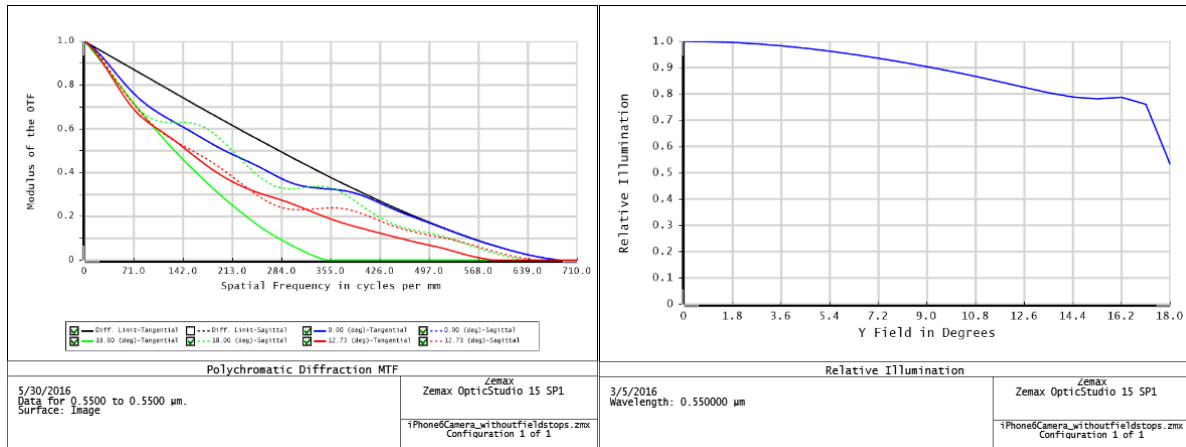Figure 9. OPD Fans and Wavefront Map

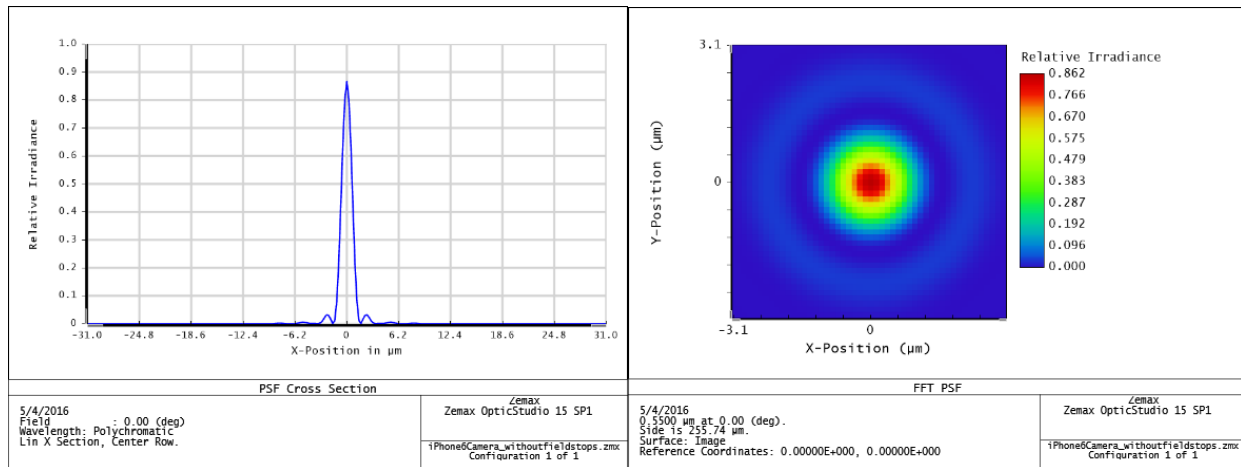Figure 10. MTF and Relative Illumination

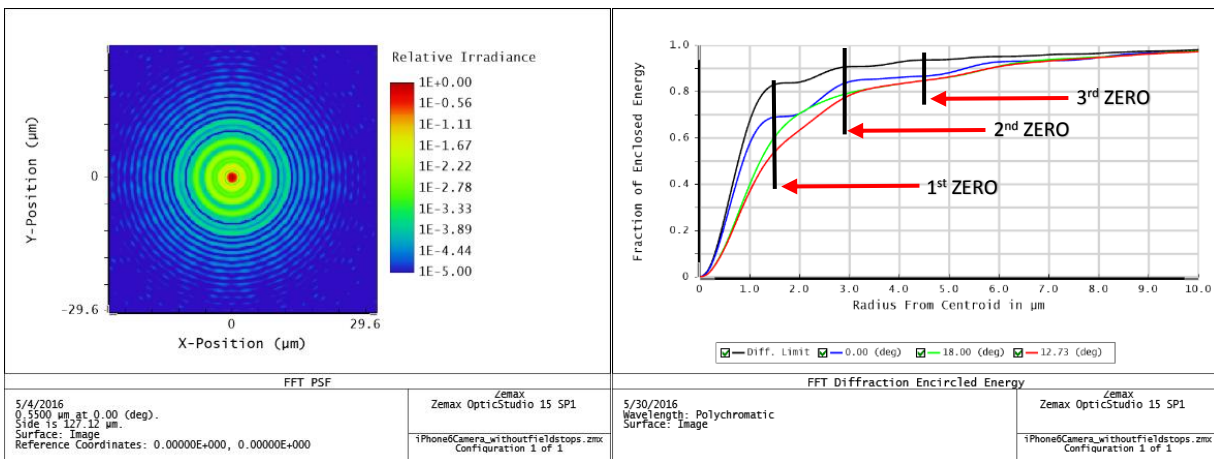Figure 11. PSF Cross Section and Linear PSF at Image Plane

Figure 12. Log PSF at Image Plane and Encircled Energy

IV. MECHANICAL MODEL

The lens barrel was designed in SolidWorks from an exported *.STP file of the optical prescription. The lens barrel, a variation of a monolithic clamshell, was designed using best known methods for plastic mold injected optics and is made of a readily available plastic-PBT. Best known methods were used since no literature regarding the mechanical barrel design was found. The extrema ray bundles, shown in figure 5, represent the FOV of the camera and were also exported in the *.STP file to ensure that the barrel design did not unintentionally vignette any rays.

It is common for plastic lenses to be made with flanges at the edges so that these features can be used as mounting points in the lens barrel and also serve as datums for alignment. In SolidWorks, the flanges were designed for each lens to allow a clearance of 10% of the lens surface clear aperture to reduce hoop and contact stresses induce into the optic from this mount [6]. Once the lens barrel was designed around the lenses, the lenses were deleted because SolidWorks is unable to recognize the 14th order aspheric terms, rather, it uses a cubic spline feature recognition which poorly fits to an aspheric surface. The lenses were later imported to FRED.
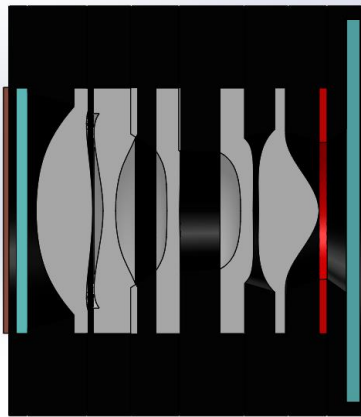
Figure 13. SolidWorks Assembled System

Before the CAD file was exported to FRED, it was discovered that an effective way to control the stray light contribution of each surface within the lens barrel is to segment the barrel into optical spaces [24]. This method of segmentation is a useful trick when stray light mitigation is required, specifically, when importance sampling comes into play. Additionally, the understanding of how different optical spaces contribute to stray light can be looped back to the design and manufacturing processes so that a mitigation strategy can be employed. The segmented lens barrels are shown in figure 14.

Figure 14. SolidWorks (left) and FRED Segmented Lens Barrel

V. CRITICAL, ILLUMINATED & COMMON OBJECTS

Critical and illuminated objects are important features to recognize within an optical system because they identify which surfaces will contribute to first order stray light. By definition, a critical object is any object which the detector can see while looking towards the universe. Conversely, illuminated objects are objects which the universe can see while looking towards the detector. Objects which are both critical and illuminated are known as common objects an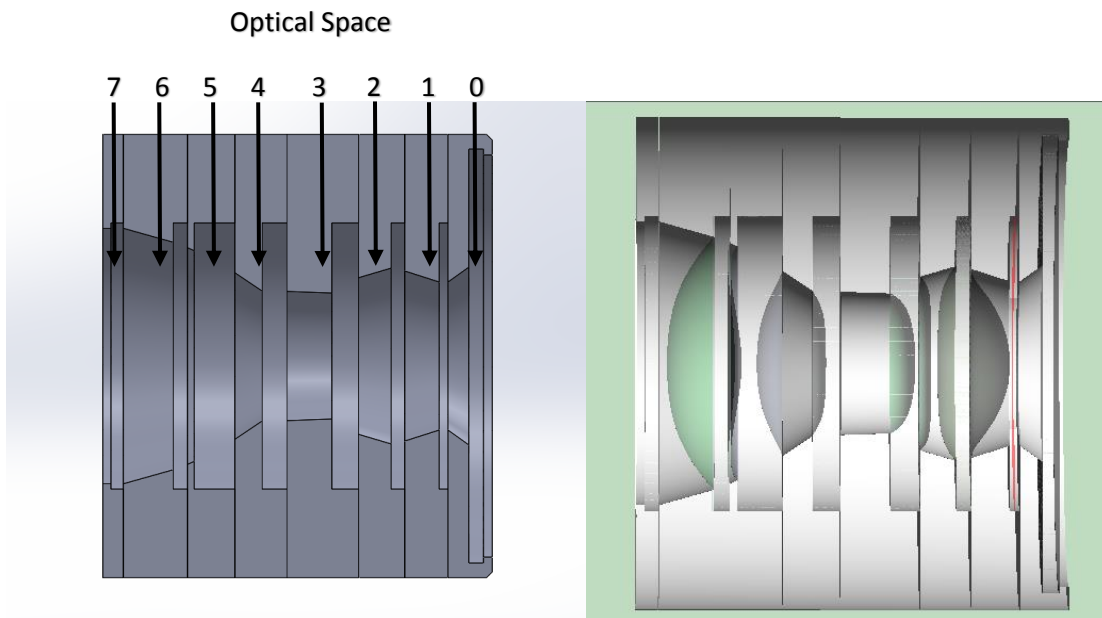d potential first order stray light sources. This implies that all surfaces of optical elements are common objects because, by design, they see both critical and illuminate objects.

To determine the critical and illuminated objects, a non-sequential forward and reverse ray trace is performed, respectively. The specific details of critical and illuminate objects recognition are below. Note that all scattering models were turned off to ensure that scattered rays were not contributing to the identification of the critical and illuminated objects. In addition, all ray trace controls were configured to only transmit the specular ray.

CRITICAL OBJECTS

To determine these critical objects, a non-sequential reverse ray trace, starting just off the surface of the detector, was performed in FRED. This involved placing a Lambertian source 0.001mm from the surface of the detector and tracing one million rays backwards through the system. In addition, all ray trace controls were configured to only transmit the specular ray. The exact details of the source are shown in table 6. Notice that the rays propagate at ±45° because the source was place 5mm in front of the optical system. If the source were to be placed the entrance pupil of the system then the rays would have to propagate at ±90°.

Ray Position		Ray Directions	
Surface	Image Plane	Type Name	Random Directions into an °range
Type Name	Random Surface	Rays	1
Rays	1,000,000	Outer Semi-Aperture	45° for X & Y
Direction	Use Dir. Function	Hole Inner Aperture	0 for X & Y
Offset	-0.001mm	Source Type	Lambertian
Iteration	No	Shape	Circular
Reverse Ray Direction?	Yes	Forward Direction	(0, 0, 1)
		Local X Direction	(1, 0, 0)

Table 6. Critical Source Parameters

Ray Count	Power	Element	Surface
7318	0.006226	Lens 2	Bevel 1
43844	0.038842	Lens 3	Bevel 1
6368	0.006349	IR Filter	Edge
386	0.000341	Lens 4	Edge
830	0.000735	Lens 4	Bevel 2
13299	0.013034	Lens 5	Bevel 2
301	0.000241	Aperture Stop	Inner Wall
242	0.000193	Barrel	Optical Space 0: TrimSurf 22
6216	0.004977	Barrel	Optical Space 1: B-Spline Surface 4
6308	0.005051	Barrel	Optical Space 1: B-Spline Surface 5
304	0.000248	Barrel	Optical Space 1: TrimSurf 31
6841	0.005704	Barrel	Optical Space 2: B-Spline Surface 3
6867	0.005725	Barrel	Optical Space 2: B-Spline Surface 22
30261	0.026273	Barrel	Optical Space 3: B-Spline Surface 2
1385	0.001202	Barrel	Optical Space 3: TrimSurf 12
30296	0.026303	Barrel	Optical Space 3: B-Spline Surface 31
106778	0.096482	Barrel	Optical Space 4: B-Spline Surface 2
55986	0.051443	Barrel	Optical Space 4: TrimSurf 12
106247	0.096002	Barrel	Optical Space 4: B-Spline Surface 31
2602	0.002439	Barrel	Optical Space 5: B-Spline Surface 2
231	0.000204	Barrel	Optical Space 5: B-Spline Surface 4
92	8.03E-05	Barrel	Optical Space 5: TrimSurf 12
290	0.000256	Barrel	Optical Space 5: B-Spline Surface 13
2629	0.002485	Barrel	Optical Space 5: TrimSurf 30
2679	0.002509	Barrel	Optical Space 5: B-Spline Surface 31
94618	9.27E-02	Barrel	Optical Space 6: B-Spline Surface 3
94714	0.092829	Barrel	Optical Space 6: B-Spline Surface 22
32952	0.032296	Barrel	Optical Space 6: TrimSurf 30
16406	0.016405	Barrel	Optical Space 7: B-Spline Surface 2
6994	0.006972	Barrel	Optical Space 7: B-Spline Surface 3
165677	0.165676	Barrel	Optical Space 7: TrimSurf 21
5999	0.005982	Barrel	Optical Space 7: B-Spline Surface 22
6669	0.006668	Barrel	Optical Space 7: TrimSurf 30
16600	0.016599	Barrel	Optical Space 7: B-Spline Surface 31

Table 7. Critical Objects

ILLUMINATED OBJECTS

To determine the illuminated objects, a non-sequential forward ray trace, starting from the object plane, was performed in FRED. This involved placing a source at the object plane and tracing one million rays forward through the system. The exact details of the source are shown in table 8. Notice that the rays propagate at ±20° and not ±90° because when the source was placed at the detector any rays

outside of ±20° would vignette and not propagate through the optical system and would be computationally inefficient.

Ray Position		Ray Directions	
Surface	Object Plane	**Type Name**	Random Directions into an °range
Type Name	Random Surface	**Rays**	1
Rays	1,000,000	**Outer Semi-Aperture**	20° for X & Y
Direction	Use Dir. Function	**Hole Inner Aperture**	0 for X & Y
Offset	0.001mm	**Source Type**	Lambertian
Iteration	No	**Shape**	Circular
Reverse Ray Direction?	No	**Forward Direction**	(0, 0, 1)
		Local X Direction	(1, 0, 0)

Table 8. Illuminated Source Parameters

Ray Count	Power	Element	Surface
1	8.51E-07	Lens 3	Edge
71	6.04E-05	Lens 3	Bevel 1
2443	0.002078	Lens 4	Bevel 2
2834	0.002315	Lens 5	Bevel 2
71348	0.069928	Aperture Stop	Back Face
1286	0.00126	Aperture Stop	Inner Wall
3582	0.003581	Barrel	Optical Space 0: B-Spline Surface 3
35540	0.034832	Barrel	Optical Space 0: B-Spline Surface 5
339581	0.336185	Barrel	Optical Space 0: TrimSurf 13
35192	0.034491	Barrel	Optical Space 0: B-Spline Surface 14
68527	0.067163	Barrel	Optical Space 0: TrimSurf 22
71304	0.071303	Barrel	Optical Space 0: TrimSurf 31
3585	0.003584	Barrel	Optical Space 0: B-Spline Surface 32
23	2.25E-05	Barrel	Optical Space 1: B-Spline Surface 4
37	3.63E-05	Barrel	Optical Space 1: B-Spline Surface 5
912	0.000893	Barrel	Optical Space 1: TrimSurf 13
126030	0.123522	Barrel	Optical Space 1: TrimSurf 22
33	3.11E-05	Barrel	Optical Space 2: B-Spline Surface 3
10	9.60E-06	Barrel	Optical Space 2: TrimSurf 21
33	3.11E-05	Barrel	Optical Space 2: B-Spline Surface 22
1027	0.000928	Barrel	Optical Space 3: B-Spline Surface 2
43	3.97E-05	Barrel	Optical Space 3: TrimSurf 30
1031	0.000932	Barrel	Optical Space 3: B-Spline Surface 31
4203	0.003648	Barrel	Optical Space 4: B-Spline Surface 2
6	5.11E-06	Barrel	Optical Space 4: B-Spline Surface 3
2	1.70E-06	Barrel	Optical Space 4: B-Spline Surface 22
1406	0.001245	Barrel	Optical Space 4: TrimSurf 30
4318	0.003748	Barrel	Optical Space 4: B-Spline Surface 31

Ray Count	Power	Element	Surface
685	0.000571	Barrel	Optical Space 5: B-Spline Surface 2
2240	0.001878	Barrel	Optical Space 5: TrimSurf 12
667	0.000556	Barrel	Optical Space 5: B-Spline Surface 31
949	0.000764	Barrel	Optical Space 6: B-Spline Surface 3
2029	0.001658	Barrel	Optical Space 6: TrimSurf 21
1042	0.000839	Barrel	Optical Space 6: B-Spline Surface 22
1459	0.001145	Barrel	Optical Space 7: B-Spline Surface 2
115	9.03E-05	Barrel	Optical Space 7: TrimSurf 12
2201	0.001744	Barrel	Optical Space 7: TrimSurf 30
1470	0.001153	Barrel	Optical Space 7: B-Spline Surface 31

Table 9. Illuminated Objects

The following table is a list of objects which are both illuminated and critical- common objects. By default, all surfaces of the optics are common objects because the detector must look through them to see the universe. However, FRED knows this and excludes these surfaces which is why they do not appear in the table below even though they are considered common objects. The next task is to apply coating and scatter models to these surfaces so that their contribution to stray light can be analyzed.

Element	Optical Space	Surface
Aperture Stop	1	Inner Wall
Lens 3	4	Bevel 1
Lens 4	5	Bevel 2
Lens 5	6	Bevel 2
Barrel	0	TrimSurf 22
Barrel	1	B-Spline Surface 4
Barrel	1	B-Spline Surface 5
Barrel	1	TrimSurf 31
Barrel	2	B-Spline Surface 3
Barrel	2	B-Spline Surface 22
Barrel	3	B-Spline Surface 2
Barrel	3	B-Spline Surface 31
Barrel	4	B-Spline Surface 2
Barrel	4	B-Spline Surface 31
Barrel	5	B-Spline Surface 2
Barrel	5	TrimSurf 12
Barrel	5	B-Spline Surface 31
Barrel	6	B-Spline Surface 3
Barrel	6	B-Spline Surface 22
Barrel	7	B-Spline Surface 2
Barrel	7	TrimSurf 30
Barrel	7	B-Spline Surface 31

Table 10. Common Objects

VI. COATING & SCATTER MODELS

With the common objects now known, coating and scatter models can be applied to these surfaces. Many of the coating specifications for the iPhone 6 camera are considered proprietary information and thus unknown. However, it is reasonable to assume that in place of the exact coating specifications, common industry coating specifications can be applied. The same holds true for the surface roughness specifications for both the optics and structure. The specific coating and scatter models will be covered in the coming sections.

COATING MODELS

Coating models were applied to the window, lenses, filter, detector and structure. The exact coating specification for each optic is listed in table 11. For reference, these models were all built with 550nm as the reference wavelength.

Element(s) Affected	Coating Type	Coating Specifications
Glass Window/ IR Filter	AR (thin film)	99%T & 1% R
Plastic Lenses	AR (thin film)	98% T & 2% R
Detector	AR (Al)	80% T & 20% R
Structure	Bare	93% A & 7% R

Table 11. Coating Model Specs

According to Baumer, AR coatings on plastic optics can achieve values of 0.25%R using a 12 quarter-wave (QW) layer when applied with the AR-hard® coating deposition process [4]. However, the number of deposition layers is linearly proportional to the cost of the coating [5] which implies that this technique is rather costly therefore a more conservative 2% reflectivity value will be used for the plastic lenses. Additionally, coating technology for glass optics is much more mature, therefore, a 99% reflectivity coating was determined to be an easily achievable value for the window and IR filter [15].
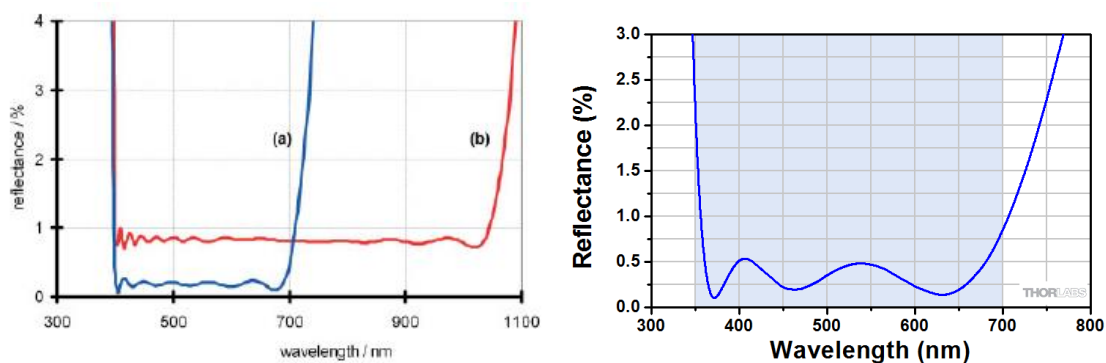

Figure 15. Plastic (left) and Glass (right) Optic Coatings

Schulz demonstrates that the reflectance of uncoated PMMA at normal incidence is roughly 7% across the entire visible spectrum [16]; the other 93% is absorbed. These absorption and reflectance values were then used to build the structure coating model.
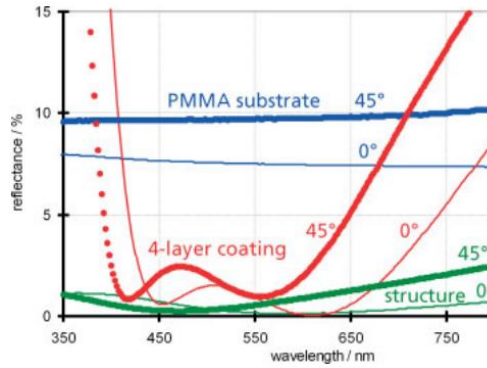
Figure 16. Structure (left) and Detector (right) Coatings

The iPhone6 camera sensor, known as the iSight, is a CMOS detector with 8 megapixels and 1.5μm pixel pitch which yields a 4.25 mm² square array. The exact coating specifications for this sensor are unknown but common coating specifications for sensors were used [17]. To be on the ultra-conservative side, a value less than the uncoated transmittance will be used for the sensor surface. It was assumed that a 20% reflectance would be a good ultra-conservative value.
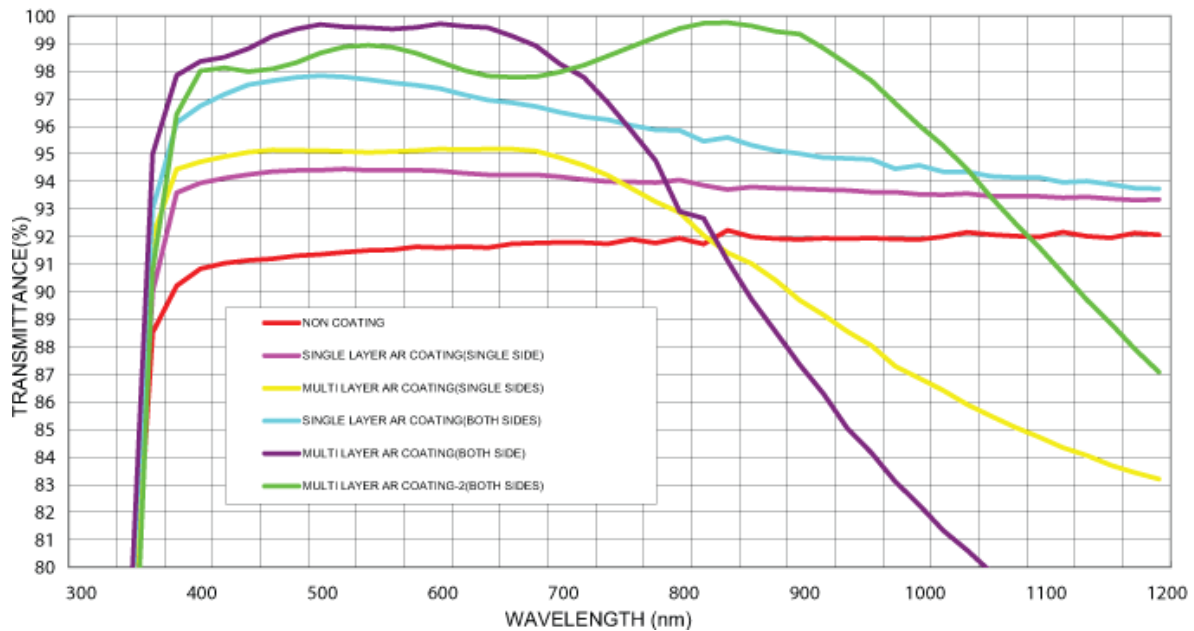

Figure 17. Sensor Coating

The uncoated transmission spectra for PMMA, PC and COP plastics are listed in figure 18. Although, the lens barrel is made from the PBT polymer it has similar reflection properties of these three polymers and will serve as the reference for the bare, uncoated, reflectance properties of the lens barrel material.
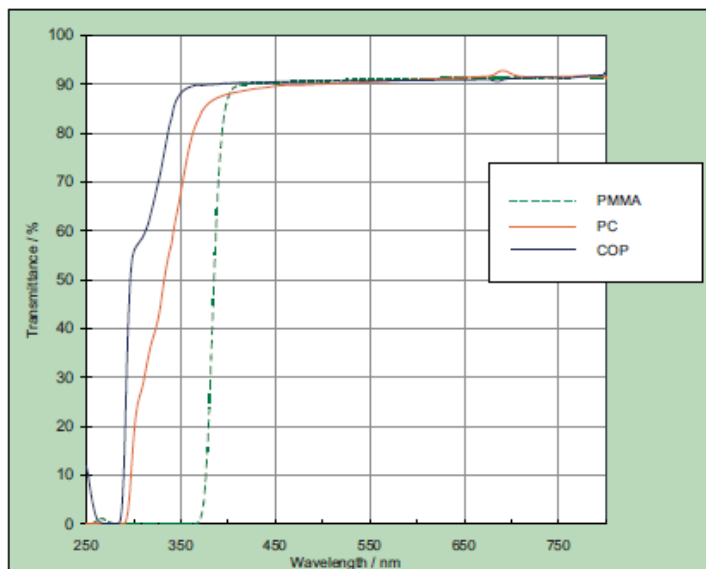
Figure 18. Transmission Spectra of Plastics

Next, these coating properties were then used to build coating models for each element in FRED. A screenshot of this interface is shown in figure 19. The wavelength, reflectivity and transmission data were the only variables used for this coating model.
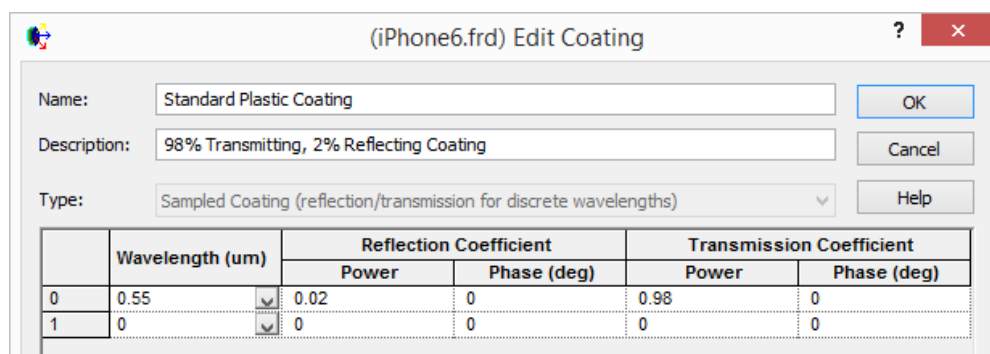

Figure 19. FRED Coating Model

SCATTER MODELS

The following scatter models were used to produce scattered rays in FRED. Note that the contamination mechanism effects all elements.

Elements	Scatter Mechanism	Scatter Model
Windows/Lenses/Filters	Surface Micro-roughness	Harvey Shack
Structure	Surface Micro-roughness	Flat Black Paint (4.5%R at NI)
All	Surface Contamination	MIE w/MIL-1246C density function

Table 12. Scatter Model Specs

HARVEY-SHACK MODEL

The Harvey-Shack model is useful for smooth surfaces. Therefore, in order for the Harvey-Shack model to be valid, the optical elements must satisfy the smooth surface criterion (SSC). The smooth surface criterion is stated in equation 6.

$$2\pi\Delta n\sigma \ll \lambda \qquad (6)$$

where Δn is the change in refractive index between the material and the incident medium, σ is the surface roughness and λ is the wavelength. Fest points out that a common and easily achievable surface roughness for a plastic optic is 40Å [18]. For this surface roughness, the 550nm reference wavelength and the index values stated in table 13, the smooth surface criterion was calculated for each material. As shown in table 13, all three materials satisfy the smooth surface criterion therefore the Harvey-Shack model may be used as the scatter model.

Another concept used for scatter models is the total integrated scatter (TIS). TIS is described as the total scatter from a surface integrated over 2π steradians. The integration of the BSDF across all the scatter angles yields the TIS, for a given angle of incidence. The TIS for each optical element was calculated at normal incidence according to equation 7 and the results are listed in table 13.

$$TIS = \left(\frac{2\pi\Delta n\sigma\cos(\theta_i)}{\lambda}\right)^2 \qquad (7)$$

Elements	Material	Index of Refraction	SSC (nm)	b_0	TIS (%)
Window	Sapphire	1.7715	0.194	0.1099	0.1243
L1 & L4	TOPAS®	1.544	0.137	0.05465	0.0618
L2, L3, & L5	Udel®	1.632	0.159	0.0738	0.0834
IR Filter	N-BK7	1.5168	0.130	0.04935	0.0558

Table 13. Total Integrated Scatter Values

Next, the BSDF for the Harvey-Shack model needs to be developed. The BSDF model is described by the empirically derived coefficients b_0, l and s, the angle of incidence θ_i and the scatter angle θ_s. In a $|\beta-\beta_0|$ BSDF scatter plot, l (known as the "knee") is described as the location at which the plot bends. The coefficient s is described as the slope and b_0 is the maximum value, as shown in figure 20. The BSDF is described by equation 9.
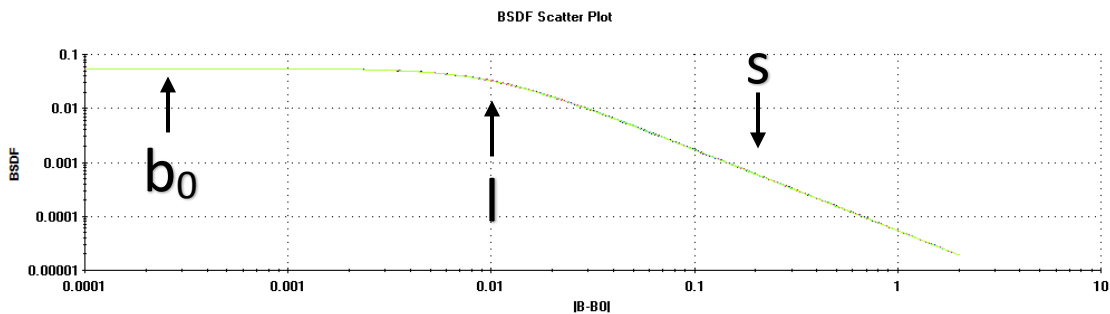

Figure 20. $|\beta-\beta_0|$ BSDF Plot

$$BSDF = b_0 \left\{ 1 + \left[\frac{|\sin(\theta_i) - \sin(\theta_S)|}{l} \right]^2 \right\}^{s/2} \tag{9}$$

Additionally, b_0 is calculated based on index of refraction, surface roughness, wavelength and the s and l coefficients, according to equation 10.

$$b_0 = \left[\frac{2\pi(n-1)\sigma}{\lambda} \right]^2 \left(\frac{1}{2\pi} \right) (s+2) l^s \left[\frac{1}{(l^2+1)^{(s+2)/2} - (l^2)^{(s+2)/2}} \right] \tag{10}$$

According to Fest, for a smooth plastic surface, common values are l = 0.01, s=-1.5 [18]. Applying these concepts, the more intuitive angular BSDF scatter models were generated in FRED. Note that at the specular angle the BSDF is maximum. From a conservation of energy point of view, it can be understood that energy is conserved along the ray path of the specular ray. The angular scatter model can be converted from the|β-β₀| scatter model but these details are not of importance to this section.
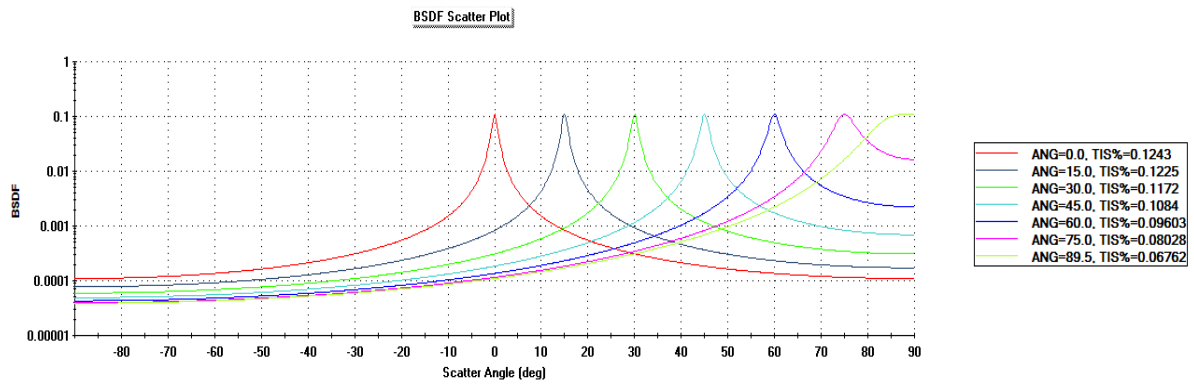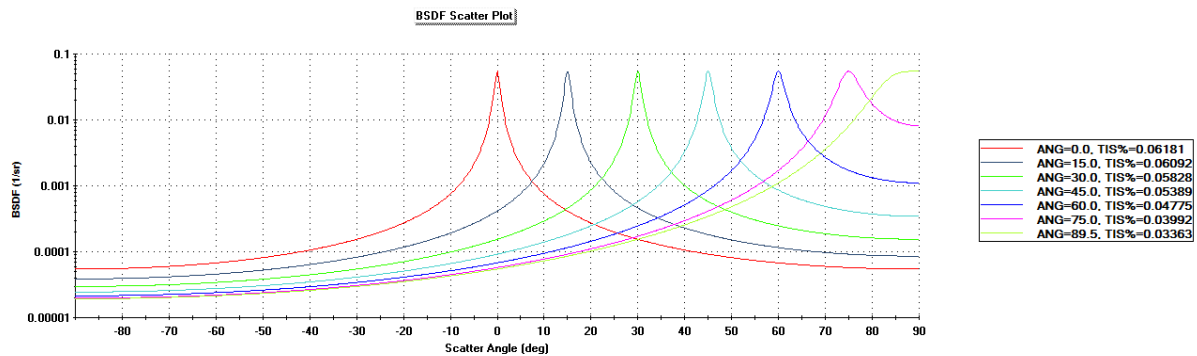

Figure 21. Sapphire Scatter Model

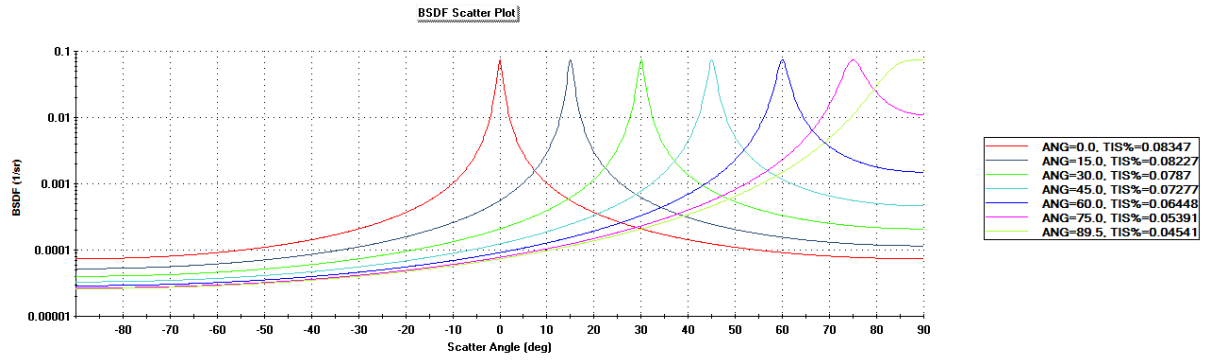Figure 22. TOPAS® 5013 Scatter Model
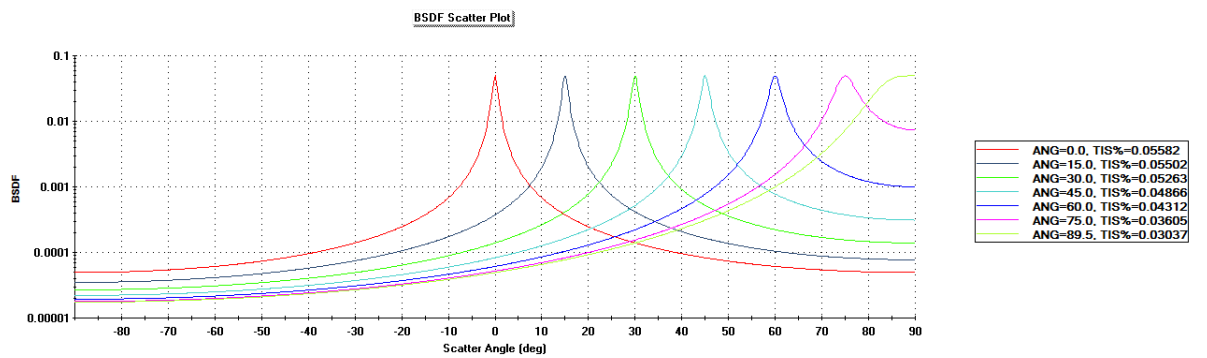
Figure 23. Udel® P-1700 Scatter Model

Figure 24. N-BK7 Scatter Model

Flat Black Paint

To model the scatter of the lens barrel structure, a flat black paint model was used. PBT plastic is black and will have a similar surface structure to that of flat black paint. The scatter model generated in FRED is displayed in figure 25.
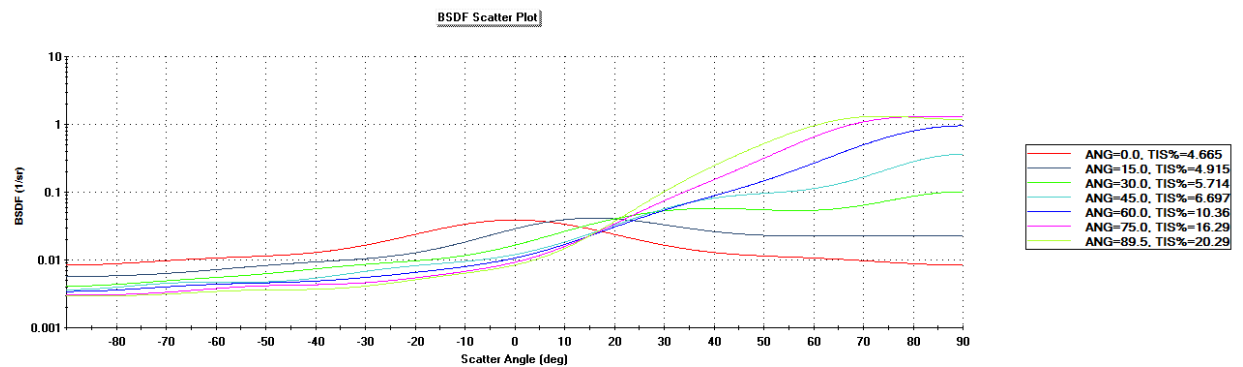

Figure 25. Uncoated PBT Scatter Model

MIE SCATTER W/ MIL-1246D DENSITY FUNCTION

Particle contamination is a major contributor to scatter. In fact, for the 40Å surface roughness, it will be demonstrated that the contamination will cause roughly the same amount of scatter. The MIL-1246D particulate density function describes the distribution of particles in terms of the number of particles per $0.1m^2$ as a function of the cleanliness level and the particle diameter, as shown in equation 11 [19].

$$log_{10}(N) = 0.926[log_{10}^2(CL) - log_{10}^2(D)] \tag{11}$$

where N is the number of particles per $0.1m^2$ greater than D microns in diameter and CL is the cleanliness level. Figure 26 plots this function in log-log space.
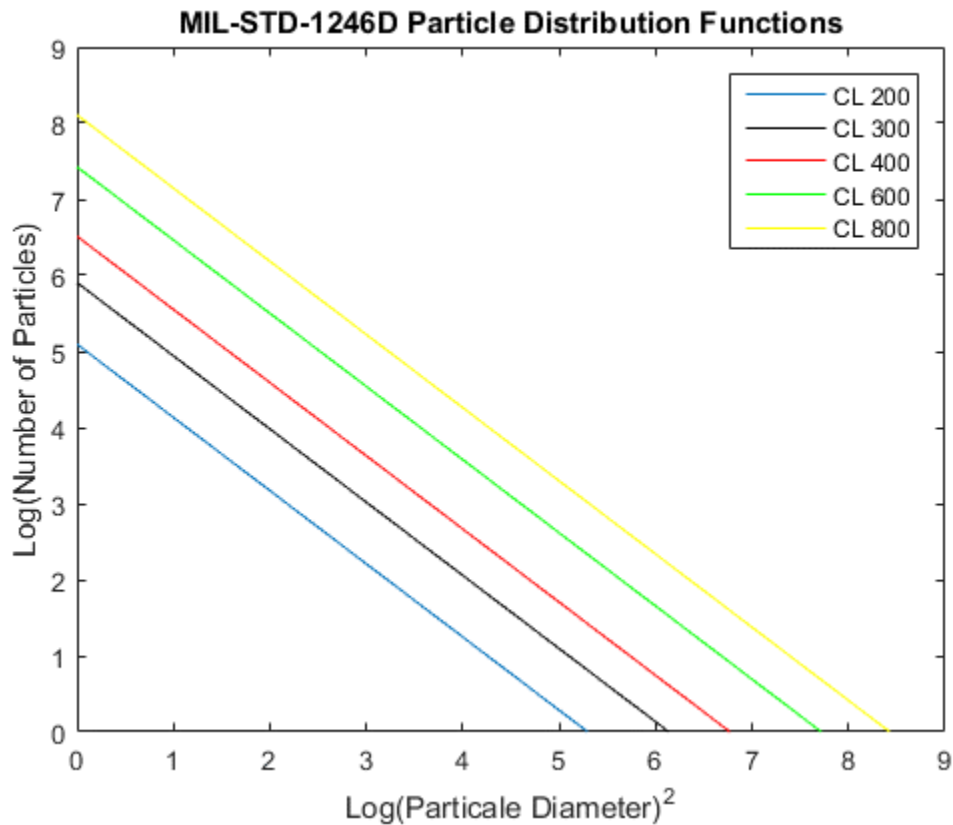

Figure 26. Contamination Particle Distributions

In order to understand the particulate contamination for different cleanliness levels in relation to the TIS the term percent area coverage (PAC) is introduced. PAC is described as the ratio of the contaminated area to the total area of the optic. As a rule of thumb, a 0.1% PAC will appear dirty to the naked eye and correlates to a cleanliness level of 396, as sown in figure 27.   It is derived that the PAC is TIS/2 due to the extinction paradox [20]. PAC can be thought of which is The PAC function is described in terms of CL in the following equation [21].

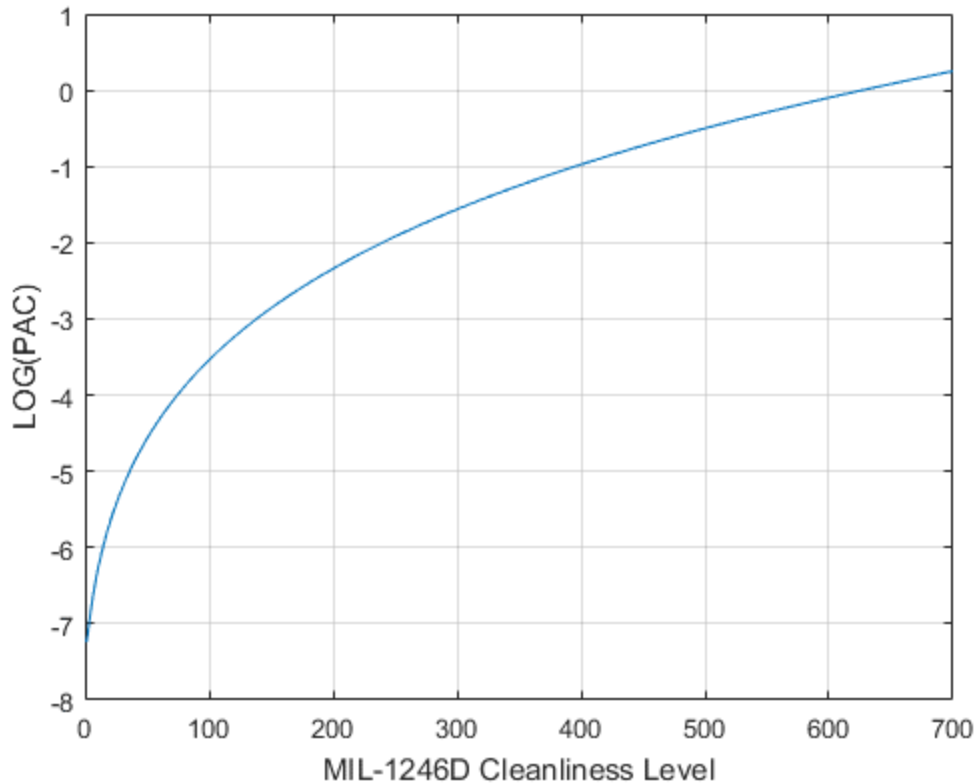$$log_{10}(PAC) = -7.245 + 0.926\, log_{10}^2(CL) \tag{12}$$

Figure 27. PAC vs. CL

The PAC provides an intuitive way to describe the particulate contamination but when modeled in FRED, PAC must be understood in terms of its optical properties. As Lindberg and Gillespie point out, the particulate contamination is able to be modeled as a complex refractive index [22].

Wavelength (µm)	Particulate Real Refractive Index	Particulate Imaginary Refractive Index
0.2	1.53	0.05
0.3	1.53	0.01
0.4	1.53	0.005
0.6328	1.53	0.0005
1.15	1.5	0.001
3.39	1.5	0.02
10.6	1.7	0.2
20	1.9	1

Table 14. Complex Refractive Index vs. Wavelength

This knowledge of particulate contamination can be applied to generate scatter models in FRED. To replicated particulate contamination introduced during the manufacturing process, for the inside of the lens barrel, a particulate contamination model was generated for a cleanliness level of 300. To replicate particulate contamination generated from the environmental a particulate contanmination model was made for a cleanliness level of 400. For an actual manufacturing environment, a contamination error budget should be built and understood. For reference, the CL 300 model represents optics inside the lens barrel and the CL 400 model represents optics outside the barrel (outer surface of window). These

scatter models were generated with the scatter model interface, where the wavelength, complex refractive index, density functions, and maximum particle diameter as variables. An example of the scatter model interface is shown in figure 28.
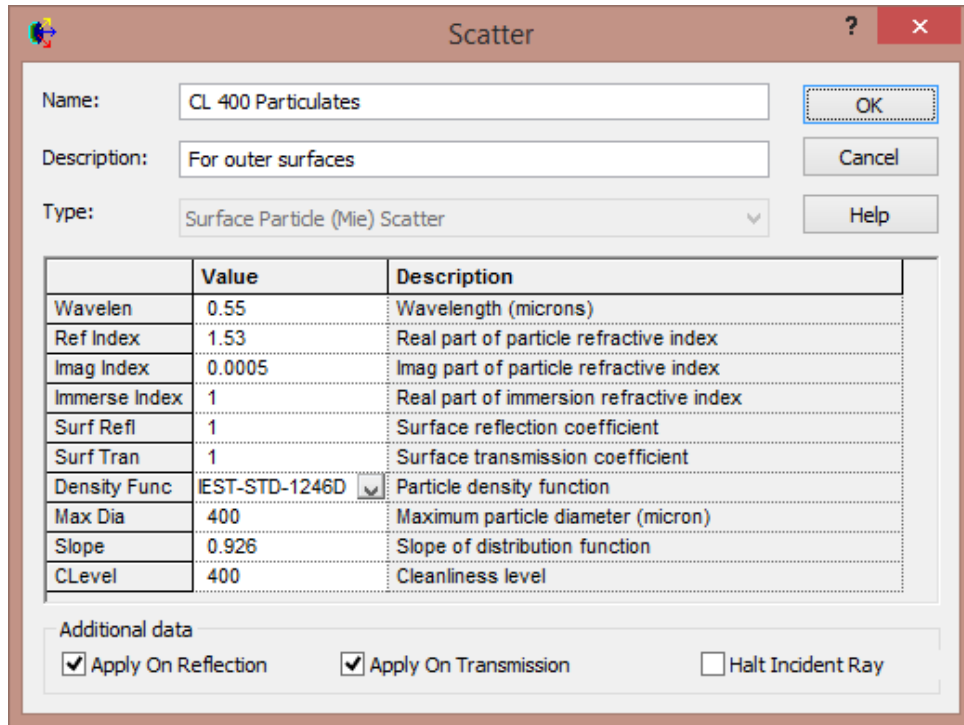

Figure 28. Scatter Model Interface

The CL 300 and CL 400 scatter models produce a Lorentzian scatter distribution under the assumption that the scatter is isotropic. In these graphs, the BSDF is plotted as a function of scatter angle for a given calculated TIS based on the angle of incidence, as shown in figures 29 and 30.
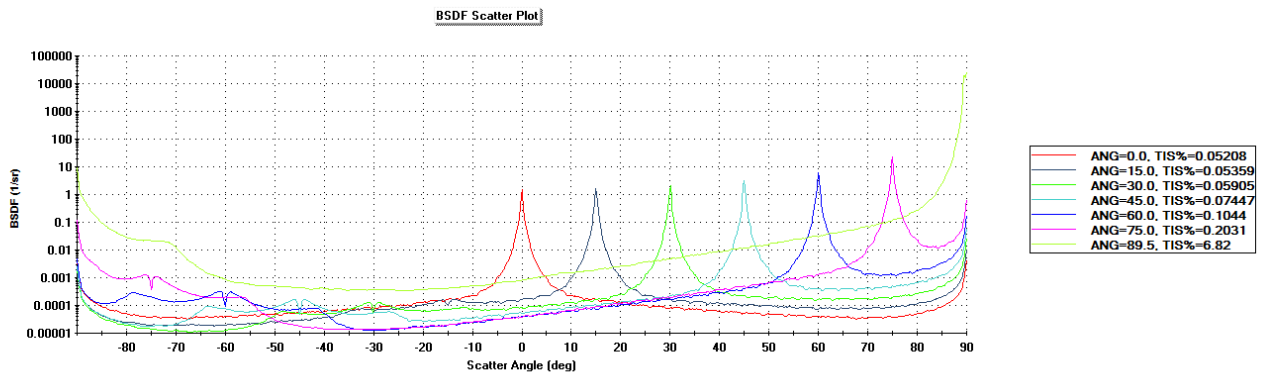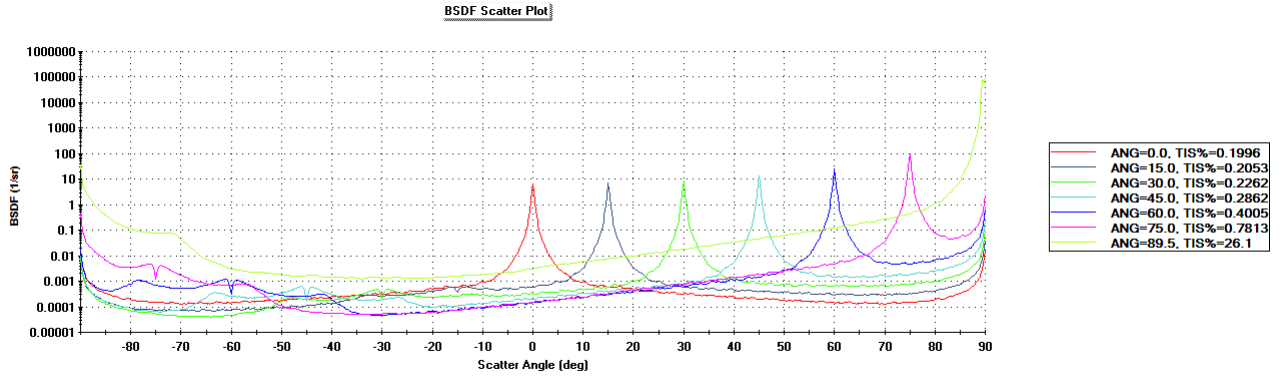

Figure 29. CL 300 Scatter Model

Figure 30. CL 400 Scatter Model

VII. IMPORTANCE SAMPLING FOR COMMON OBJECTS

Importance sampling is a method used to improve the computational efficiency of a stray light simulation for scattered rays. During the simulation, scattered rays are generated and propagate in all directions within a hemisphere. Rays which do not scatter in the direction of the detector have a probabilistic minute chance of reaching the detector. Therefore, in order to be computational efficient the rays should only be scattered in the direction of the detector. Specifically, this direction is defined as the solid angle the detector subtends from the optical surface of interest. This implies that all optical surfaces will have their own importance sampling identities, known as a curve. Furthermore, this optical surface will be reside within an optical space and anything within the same optical space will have the same importance sampling curve [23]. This makes it easier to determine the importance sampling curve for non-optical surface features such as bevels and edges. To determine the importance sampling curve for each optical space, a first order paraxial ray trace was performed in FRED results in table 14.
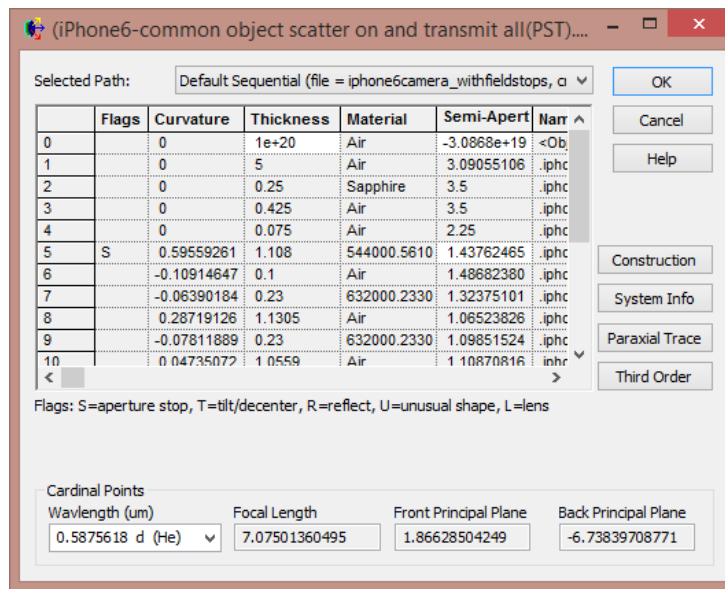

Figure 31. First Order Paraxial Raytrace

Operating under the assumption that the system is well defined by paraxial optics and the conic constants are less than 100 (verified by fig. 6) [24], the importance sampling location (ISL) and importance sampling height (ISH) can be calculated from table 15, according to equations 13 and 14.

$$ISL = \frac{-y_k}{u_{k+1}} \tag{13}$$

$$ISH = |\bar{y}_k + (\bar{u}_{k+1} * ISL)| \tag{14}$$

where y is the marginal ray height, u is the marginal ray angle, ȳ is the chief ray height and ū is the chief ray angle. Note that the paraxial ray trace does not compute values for non-optical surfaces (i.e. surfaces 0-3) and therefore they do not contain importance sampling curves. Next, the importance sampling curve is made by creating a new curve. The curve radius is the importance sampling height and the curve location is the importance sampling location with respect to the optical surface of interest. Figure 31 shows the interface in FRED where this task is performed.

Surface	y (mm)	u' (rad.)	ISL (mm)	ȳ (mm)	ū (rad.)	ISH (mm)	Semi-Aperture (mm)
0	0	1.43E-20	-	-3.08E+19	0.308683	-	3.08E+19
1	1.437624	1.43E-20	-	-1.74864	0.308683	-	3.186263
2	1.437624	9.47E-21	-	-0.20522	0.203509	-	1.642844
3	1.437624	1.43E-20	-	-0.15434	0.308683	1.471	1.591966
4	1.437624	1.43E-20	4.765	-0.02315	0.308683	0.541	1.460775
5	1.437624	-0.30168	2.706	2.22E-16	0.199924	0.787	1.437624
6	1.103363	-0.53131	3.683	0.221516	0.295531	0.102	1.32488
7	1.050232	-0.29957	3.379	0.251069	0.187298	1.757	1.301302
8	0.981332	-0.31078	5.726	0.294148	0.35906	0.269	1.27548
9	0.63	-0.17137	2.405	0.700066	0.24119	1.639	1.330066
10	0.590586	-0.262	4.348	0.75554	0.416233	0.554	1.346126
11	0.313942	-0.13582	2.049	1.19504	0.3985	2.066	1.508983
12	0.282703	-0.15325	2.525	1.286696	0.872246	0.428	1.5694
13	0.267379	-0.11198	1.316	1.37392	0.441561	0.423	1.641299
14	0.15141	-0.2032	1.130	1.831201	0.47339	-0.012	1.982611
15	0.124242	-0.13404	0.611	1.894493	0.312262	0.090	2.018736
16	0.096095	-0.2032	0.473	1.960069	0.47339	-0.043	2.056164
17	0.068602	-0.2032	0.338	2.024118	0.47339	-	2.092721
18	0.068399	-0.2032	-	2.024592	0.47339	-	2.092991

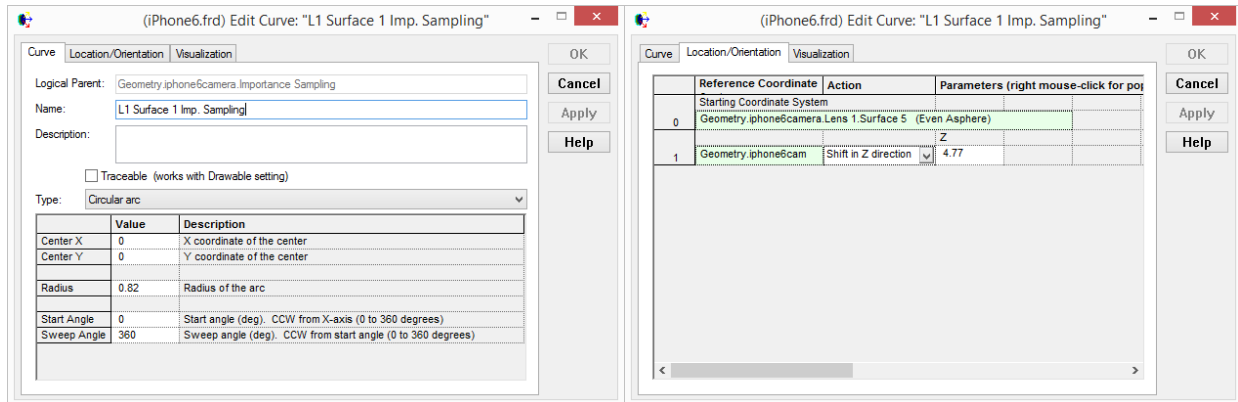Table 15. First Order Paraxial Ray Trace

Figure 32. Importance Sampling Curve

Once the importance sampling curve has been created it is applied to the surface of interest, as shown below in the FRED GUI under the scatter tab. Notice that 10 scattered rays are produce for every ray incident on this importance sampling curve.
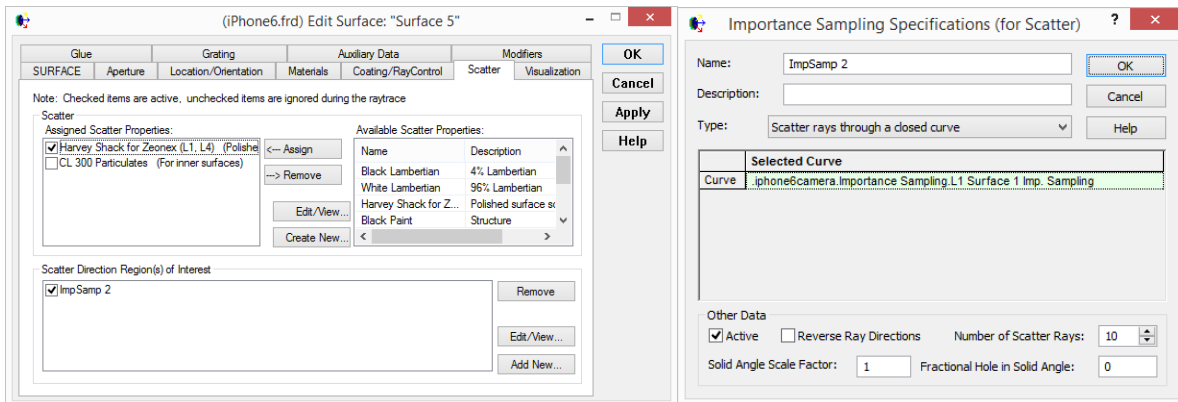

Figure 33. Applying Importance Sampling Curve

The paraxial raytrace does not compute perfect importance sampling curves therefore the size of the importance sampling curve will need to be validated. The scatter model for the surface to be validated was turned on and the scattered rays were set to be a different color than the refracted rays. A raytrace was then performed with an on-axis source, the size of the entrance pupil. To determine if the importance sampling curve size is too large or small, view the "positions spot diagram." The mouse can be dragged over the spot and the positions can be read out in the spot diagram window, as shown in figure 34. If the importance sampling curve is the correct size, the rays at the perimeter of the spot diagram should not be larger than the detector area. If they are, change the radius of the importance sampling curve and perform the raytrace again. Repeat this process until an appropriate size curve is found. Once all importance sampling curves are validated the stray light simulations can begin.
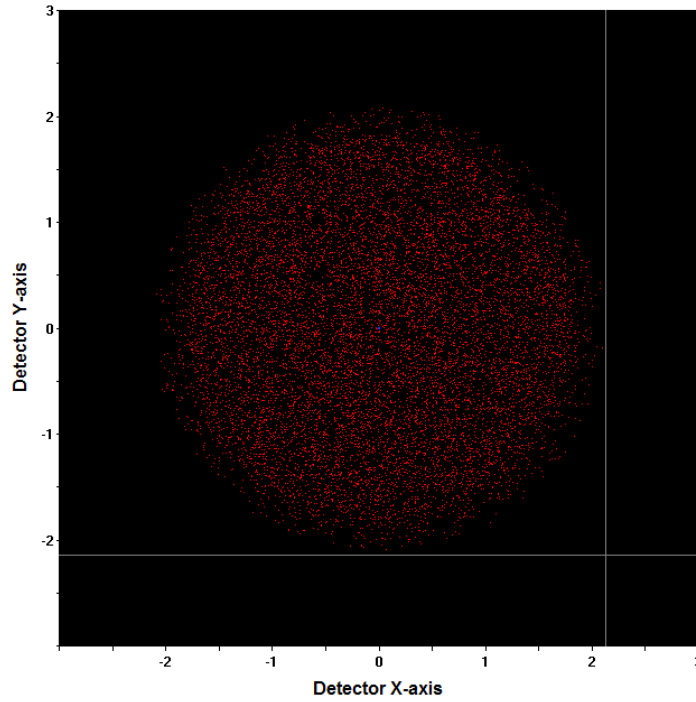
Figure 34. Detector Spot Diagram
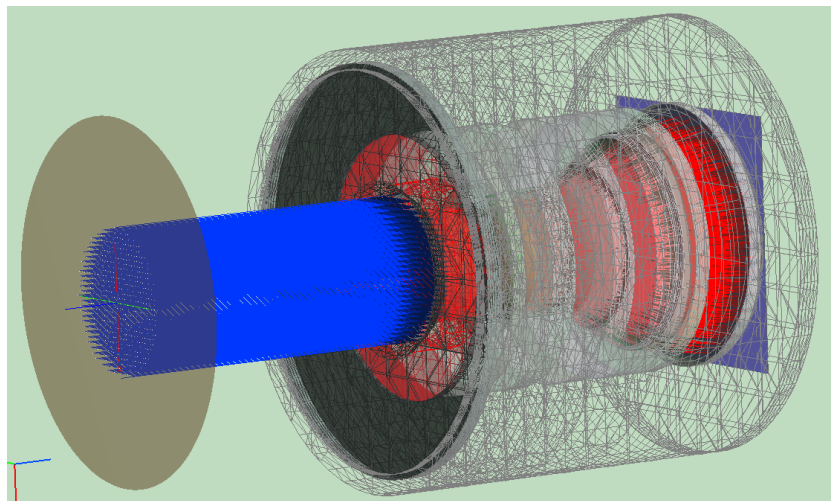
Figure 35. Ray Trace Layout for Importance Sampling

VIII. IMAGE QUALITY AFFECTS

There are many approaches to assess the image quality of the optical system, therefore, the degradative effects of stray light will be quantified differently for each stray light source. For specular components, there does not exist a quantitative method or metric to describe the image quality, rather, the overall aesthetic appearance of an image will be analyzed which can be interpreted as a Potter-Stewart method

of assessment [25]. Although, given the appearance of a ghost image, it can be interpreted that the specular components cause a localized decrease in image contrast on a region of the detector. However, given the subjective approach to this method of image quality assessment no further description or analysis will be performed. For scatter components, the image quality will degrade depending upon the spatial frequency of the surface roughness, as pointed out in table 16. As a note, the human eye tends to favor high contrast, low spatial frequencies so it will be shown that scatter components are the most detrimental to the image quality.

Common analytical methods will be introduced here to describe the effect which scattered light has on image quality.   As pointed out by Harvey and Shack, the surface transfer function (STF) can be used to describe the scattering behavior for an object with a given surface topology i.e. roughness [26]. Specifically, the STF is autocovariance of the surface topology. The autocovariance is the cross correlation of the surface topology with itself and is a mathematical tool used to reveal patterns which may be hidden by noise. This analytical method to determine the surface roughness only holds true under the following assumptions:

- The surface heights obey a Gaussian distribution.
- The surface is homogeneous and isotropic.
- The random variables produced by any two fixed pair of spatial coordinates are jointly normal i.e. the system is linear and shift invariant.

Next, by taking the Fourier transform of the autocovariance function, known as the power spectral density (PSD), insight into the scattering process can be understood from the STF [27]. The PSD relates the spatial frequencies of the surface roughness to an angular spread (scatter) of a point. That is to say, different spatial frequencies of the surface roughness correlate to different scatter characteristics and effects on image quality. In this sense, the PSD correlates to the point spread function (PSF) of a system, as described in table 16 [28].

Spatial Frequency Type	Scatter Characteristics	Image Quality
Low	Conventional Aberrations	Minor decrease in contrast & Preserves resolution
Mid	Small-Angle Scatter	Decrease resolution
High	Wide-Angle Scatter	Reduces contrast & Preserves resolution

Table 16. PSF and Image Quality

In addition to the scattered image degradation caused by the surface roughness, the image degradation inherent to the optical design must also be accounted for. Linear systems theory states that if two image degradation mechanisms are independent and uncorrelated then the system transfer function can be taken as the convolution of the diffraction and scattered PSFs [29]. The resulting product is known as the system transfer function or the composite transfer function. The linear systems theorem also states that the system transfer function can also be found by taking the product of the diffraction based transfer function and the scatter based transfer function in Fourier-space, as illustrated in figure 36. The image quality effects introduced in this section can be applied to the results of the stray light analysis in the following section. However, the surfaces under investigation are considered to have a mid and/or high spatial frequency therefore the effects of low spatial frequency content will be ignored [30].
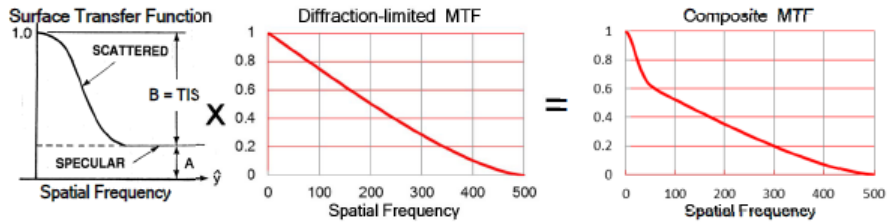
Note that the composite MTF drops very quickly to a value of 1-TIS, then continues as (1-TIS)(Diffraction-limited MTF)

Figure 36. Surface Transfer Function (STF)

IX. STRAY LIGHT ANALYSIS

Stray light analysis was performed for both specular and scatter events. Specular events were limited to monochromatic, second level events. Scatter events were limited to monochromatic, first level events. As a reminder, the mechanisms of each contributor are listed below.

Category	Mechanism
SPECULAR	Surface Reflections
	Detector Reflections
	Structure Reflections
SCATTER	Surface Micro-roughness
	Particle Contamination
	Structure Scatter

Table 17. Stray light Contributors

For reference, the nominal on-axis RMS irradiance was first calculated by setting the raytrace controls to transmit specular for the optical surfaces, halt all for all other surfaces, and setting the scatter models to off. The nominal RMS irradiance is 130,432 W/mm^2 for a unit irradiance source (4.92W/4.92mm^2). The irradiance profile shown in figure 37.
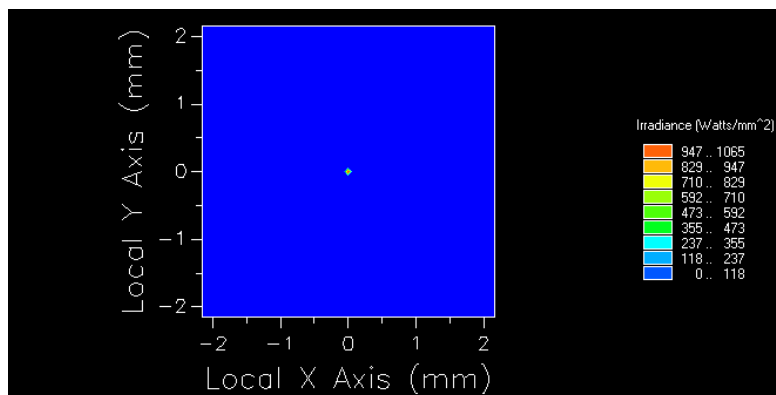

Figure 37. On-Axis Irradiance

GHOST IMAGING

This analysis examines the specular contributions to stray light caused by imperfect optical coatings. As a ray propagates through the optical system it has the potential to reflect off a refracting surface due to these imperfect optical coatings and the non-sequential propagation of light. As pointed out in table 17, specular reflections from optical surfaces, detectors and structure will be analyzed for ghost images. This analysis will only consider two surface reflections i.e. second order ghosts.
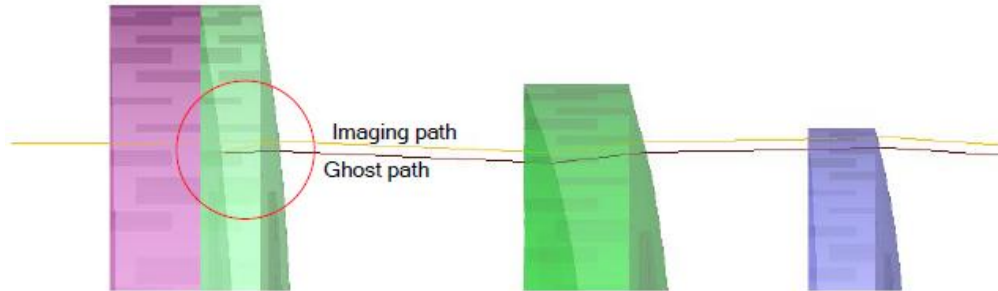

Figure 38. Ghost Path

The iPhone 6 camera consists of 15 surfaces, including the detector, therefore for two surface reflections the number of on-axis ghost paths can be expressed as:

$$\# \ ghost \ paths = n(n-1)/2 \qquad (15)$$

where n is the number of surfaces. For in-field ghosts, the number of ghost paths increases as the angle of incidence increases because more objects come into the field of view and have a high probability of reaching the detector. For out of field ghosts, the number of ghost paths decreases as the angle of incidence increases because less optical surfaces are being illuminated which decreases the probability of a ray reaching the detector. The number of ghost paths for each angle of incidence is listed in table 18.

AOI (°)	Ghost Surfaces
0	2650
5	2656
10	30778
15	10200
20	9625
25	3693
26	1019
27	9

Table 18. Ghost Paths

The optical source was a circular beam with a radius of 1.252mm which slightly overfills the entrance pupil to ensure accurate sampling of the pupil plane. Additional source parameters for this analysis are listed in table 19. Note that a random plane was selected as the ray position type to eliminate any false structure in the beam at the image plane. Additionally, the source power is a rather odd number because this is the power necessary so that the source has unit irradiance in W/mm^2.

Ray Position Type	Ray Directions Type	Power (W)	Wavelength (µm)
Random Plane	Single Direction Plane Wave	4.924459051	0.550

Table 19. Source Parameters

To analyze the ghost images of this optical system, the irradiance at the image plane was analyzed for various angles of incidence of the ray along the z-axis by perturbing the source position along the y-axis[3], as shown in figure 39. Note that ghost image analysis does not require importance sampling setup since ghost images are specular. In addition, the scatter models were turned off and the raytrace controls were set to allow all.
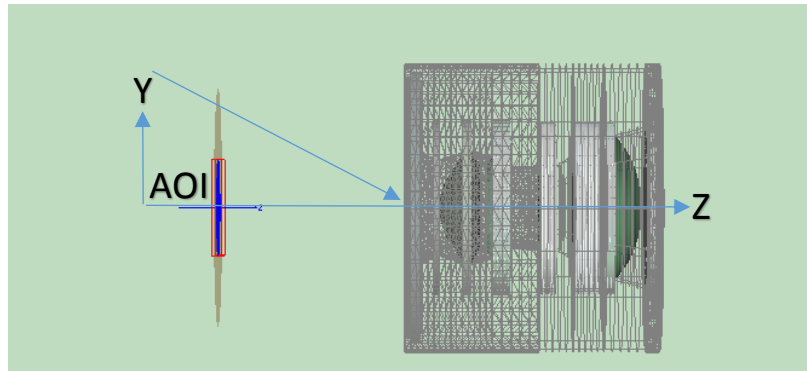

Figure 39. Source Angle of Incidence

The angle of incidence was varied until no ghosts were detected at the image plane. As the angle of incidence increases the throughput of the system will decrease which implies that the number of rays defined for the source must increase to ensure that the image plane is accurately sampled. Due to this change in the angle of incidence, a well sampled image will exhibit a bilateral symmetry about the y-axis. The exact ray sampling values used for each angle of incidence is listed in table 20.

Angle (°)	Source Rays	Generated Scatter Rays	Simulation Time (min)
0	10,000	2,653,340	15
5	20,000	2,405,620	10
10	50,000	2,519,939	8.5
15	200,000	4,796,702	13.1
20	350,000	3,538,864	7.58
25	1,000,000	5,679,231	5.75
26	1,000,000	3,049,630	1.86
27	1,000,000	2,732,193	1.12
27.175	1,000,000	2,624,093	0.96

Table 20. Ray Sampling

As Pfisterer mentions, the most detrimental ghost images are those which come to focus [31]. As a result, the normalized RMS irradiance will be the metric of choice to determine the effect a ghost image has on image quality. Ghost images effect image quality in two ways. If a ghost image has a low

---

[3] For reference, the exact ray directions are calculated in FRED using normalized direction cosines.

irradiance, large area and low power, then this will tend to decrease the image contrast/MTF. However, if a ghost image has a high irradiance, small area and high power, then this will tend to effect the resolution of the system [32]. In practice, the RMS irradiance threshold should be derived in the system requirements but for this project the top four normalized irradiance values were examined. Note that the irradiance images calculate the irradiance based on spot size of the beam on the detector and not the RMS spot size. The RMS irradiance calculation is based on the power per area as calculated from RMS spot size. Note that using RMS spot size produces a more accurate irradiance calculation because it considers the distribution of power over the detector whereas the regular spot size assumes a uniform power distribution. Due to this method of calculation, the regular spot size yields errors in the irradiance calculation, as demonstrated in figure 40. The yellow circle represents the normal spot size and the red circle represents the RMS spot size.
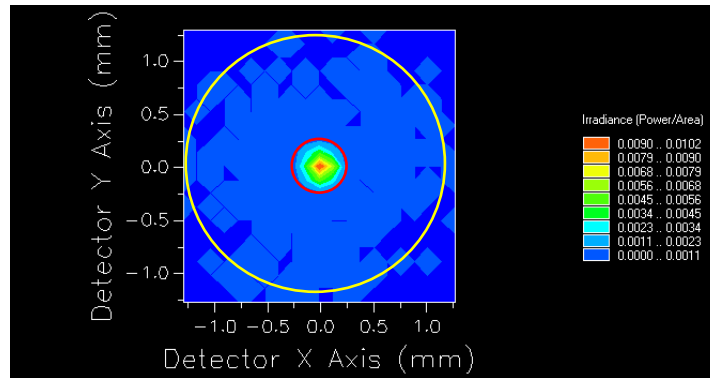

Figure 40. RMS and Non-RMS Spot

Now that the simulation and calculation methods are understood the ghost path analysis can begin. For each angle of incidence, the top four normalized irradiance values of all ghost paths were analyzed.

AOI (°)	Ray Path	RMS Irradiance (W/mm^2)	Normalized RMS Irradiance
0	0	130,432	1
0	478	9.354802972	7.17217E-05
0	479	9.352988661	7.17078E-05
0	466	1.393128597	1.06809E-05
0	467	0.341211019	2.61601E-06
5	1158	0.094694656	7.26008E-07
5	1157	0.077582875	5.94815E-07
5	1156	0.060528169	4.64059E-07
5	1160	0.015605596	1.19645E-07
10	2299	0.118851031	9.11211E-07
10	2302	0.099233339	7.60805E-07
10	2300	0.078501595	6.01858E-07
10	2303	0.072464173	5.55571E-07
15	2237	0.145029919	1.11192E-06
15	2238	0.09304392	7.13352E-07
15	27	0.064206826	4.92263E-07
15	12	0.000543492	4.16686E-09
20	26	0.020045672	1.53687E-07
20	21	0.019685929	1.50929E-07
20	11	0.017770291	1.36242E-07
20	84	0.000703999	5.39744E-09
25	15	0.024531682	1.8808E-07
25	21	0.023816372	1.82596E-07
25	13	0.01082153	8.29668E-08
25	9	0.000169909	1.30266E-09
26	6	0.013466926	1.03249E-07
26	361	2.2975E-05	1.76145E-10
26	362	1.93729E-05	1.48529E-10
26	365	8.34105E-06	6.39494E-11
27	70	0.003072682	9.18724E-07
27	69	0.005709146	5.045E-07
27	66	0.607101326	1.53019E-07
27	67	0.796453608	1.12021E-07

Table 21. RMS Irradiance

The ghost images were captured at the image plane and produced the following plots in log-base -10 space to reveal the detail. Note that the scales are different.
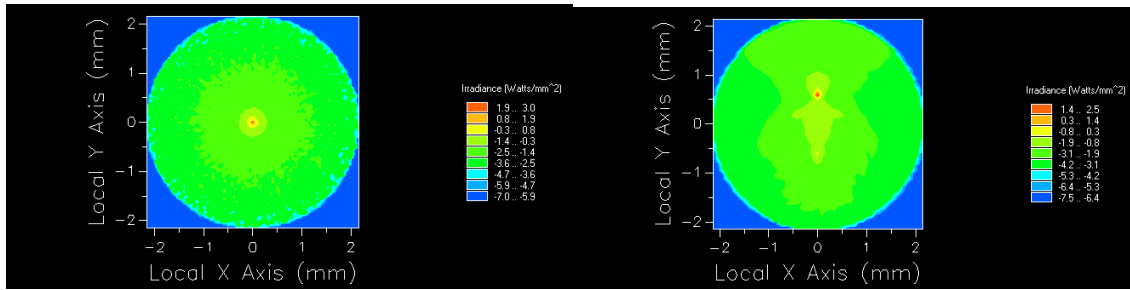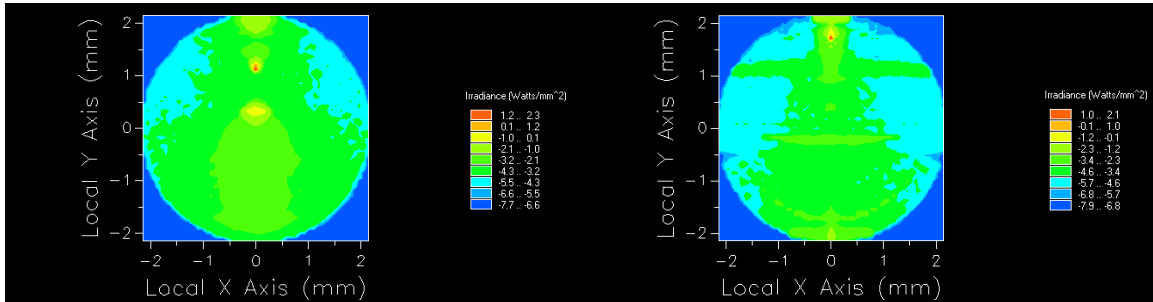
Figure 41. On-Axis and 5° Off-Axis Ghost Images Log-$_{10}$-Space
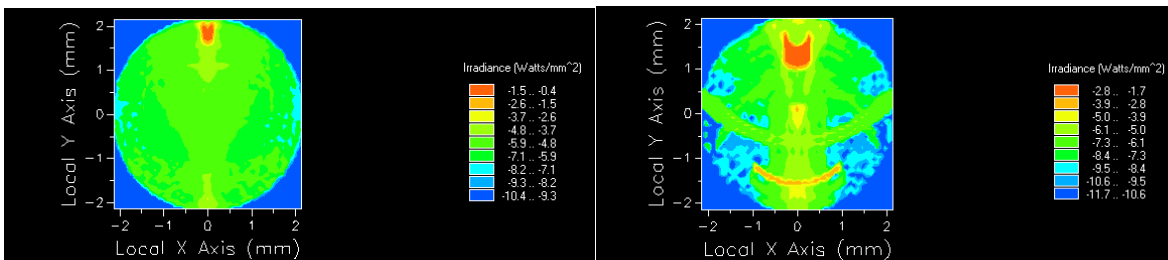

Figure 42. 10° Off-Axis & 15° Off-Axis Ghost Images Log-$_{10}$-Space

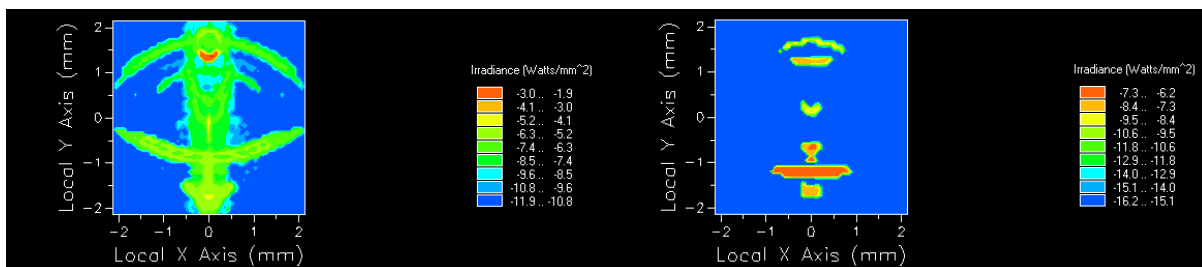Figure 43. 18° Off-Axis & 25° Off-Axis Ghost Images Log-$_{10}$-Space

Figure 44. 26° Off-Axis & 27° Off-Axis Ghost Images Log-$_{10}$-Space

For the each ghost path in table 21 the ghost surfaces were determine so that a mitigation strategy could be assigned. The analysis produced the following results.

ON –AXIS GHOSTS

For the on-axis source, all four ghost paths were caused by reflections between planar surfaces. The probability of reflections s maximized when the surfaces are planar and normal to the incident ray. The only mitigation strategy to these ghost images would be to improve the coating reflectivity properties for all of the surfaces. The ghost images in figure 45 are listed in the same order as in table 22. Note: This is the same for all ghost image sections.

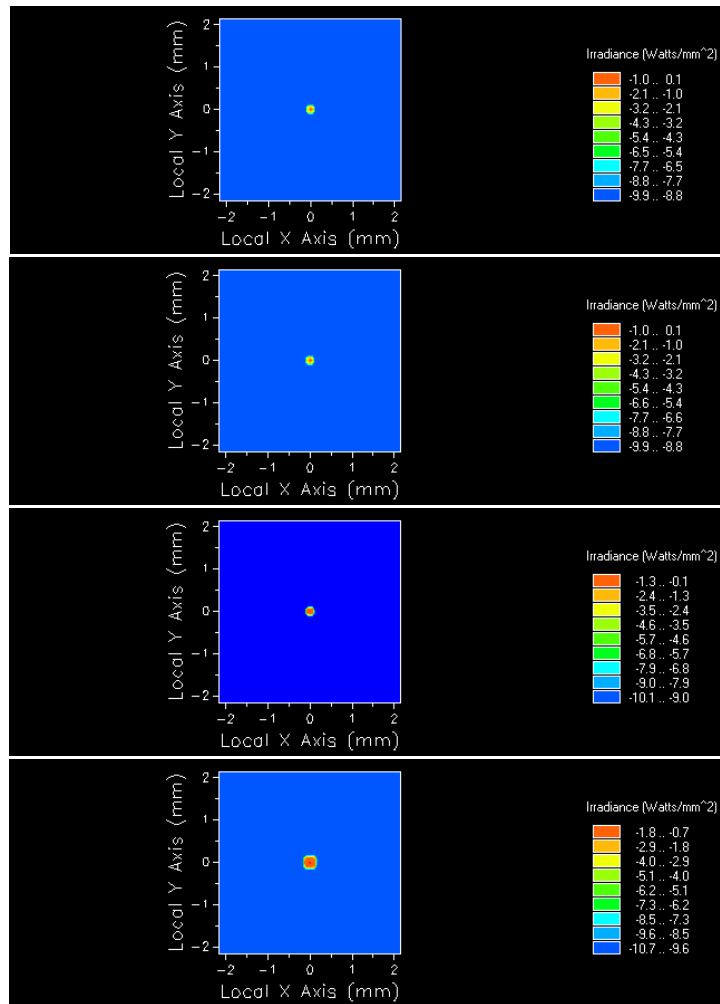| Ray Path	1st Ghost Surface	2nd Ghost Surface
478	Detector	Window Surface 2
479	Detector	Window Surface 1
466	Detector	IR Filter Surface 2
467	Detector	IR Filter Surface 1

Table 22. On-Axis Ghost Paths

Figure 45. On-Axis Ghost Images

5° OFF-AXIS GHOSTS

For the five degree off axis source, all four of the ghost paths had the detector as the first ghost surface. The detector is coated with a 20% reflectivity coating therefore one method to decrease these ghost images is to allocate a vendor who can provide a better performing detector coating. These ghost images have a small normalized RMS irradiance of one ten-millionth which may or may not be a problem depending on the system requirements. Note that there was no trend observed for the second ghosting surface therefore no mitigation strategy could be applied for these surfaces.

Ray Path	1st Ghost Surface	2nd Ghost Surface
1158	Detector	Lens 5 Surface 2
1157	Detector	Lens 5 Surface 1
1156	Detector	Lens 4 Surface 2
1160	Detector	Lens 3 Surface 2

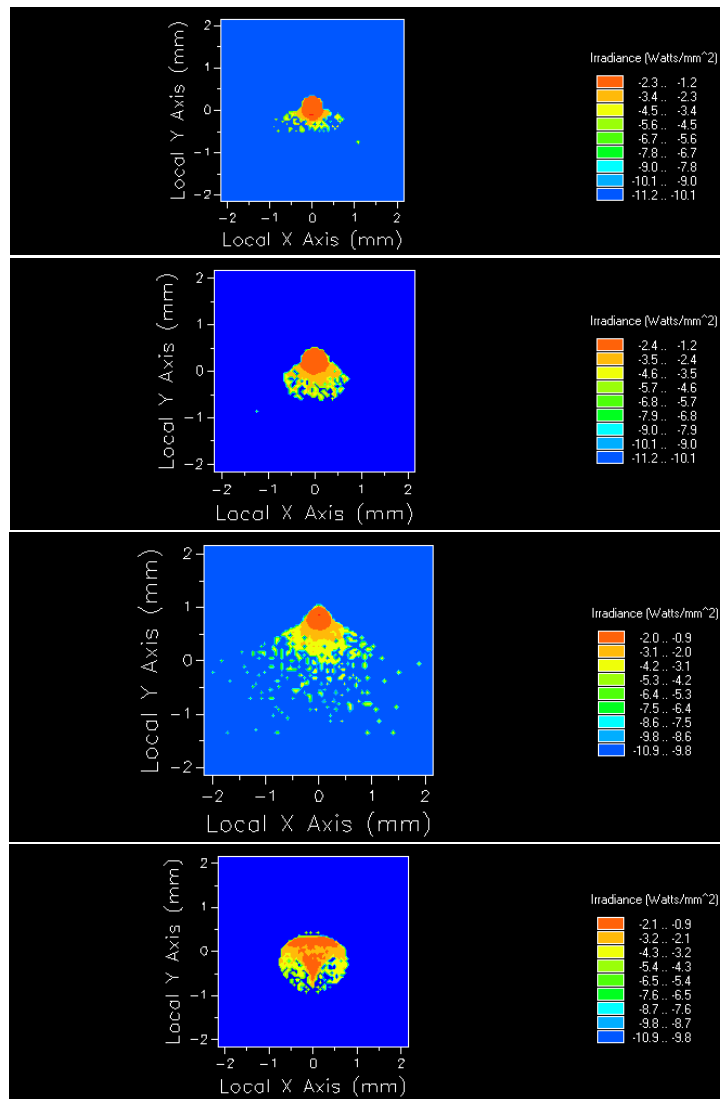Table 23. 5° Off-Axis Ghosts

Figure 46. 5° Off-Axis Ghost Images

10° OFF-AXIS GHOSTS

For the 10 degree off-axis source, the first ghost surface is the detector just like as it was for the five degree off-axis source. As a result, there are no significant changes and the mitigation strategy is the same. However, notice that for ray paths 2299 and 2300 the angular spread of these ghost images increases when compared to the previous source angle. This implies that there is more stray light per area for this source angle.

Ray Path	1st Ghost Surface	2ndGhost Surface
2299	Detector	IR filter Surface 2
2302	Detector	Lens 5 Surface 1
2300	Detector	IR filter Surface 1
2303	Detector	Lens 4 Surface 2

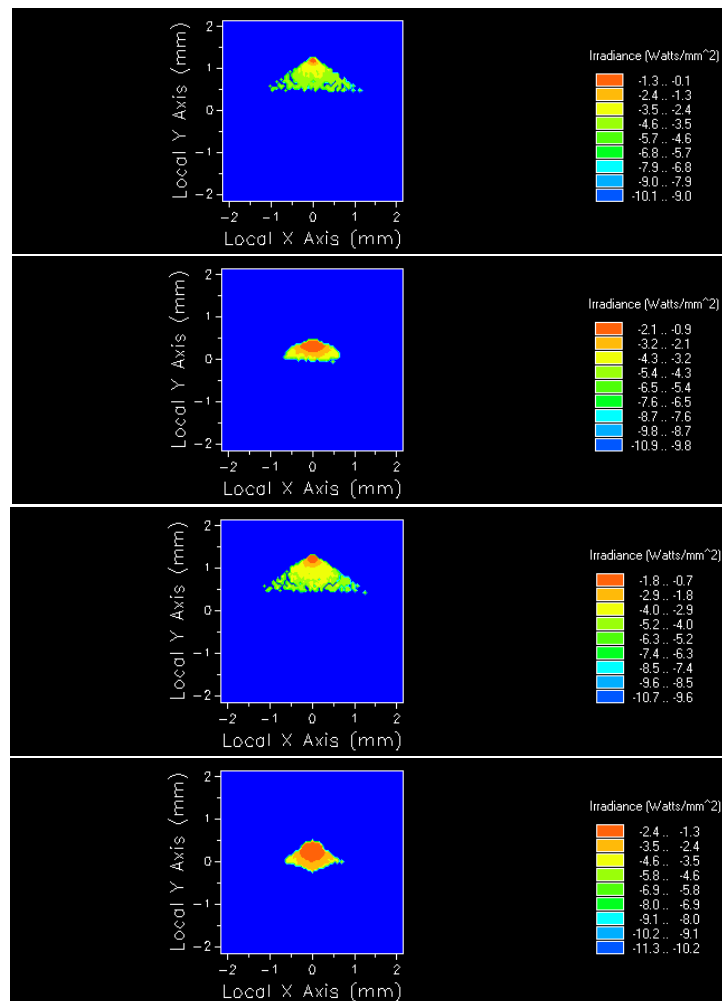Table 24. 10° Off-Axis Ghosts

Figure 47. 10° Off-Axis Ghost Images

15° OFF-AXIS GHOSTS

For the 15 degree off-axis source, the first three ghost paths are the same as the two previous source angles. However, there is an interesting observation made for this source angle. The inner wall of the aperture stop is a source of specular structure reflection. The aperture stop can only be made to a finite width and as a result this makes this surface a potential stray light source. To mitigate this issue an aperture stop with a smaller width should be used.

Ray Path	1st Ghost Surface	2ndGhost Surface
2237	Detector	IR filter Surface 2
2238	Detector	IR filter Surface 1
27	Detector	Lens 5 Bevel 2
12	A.S. Inner Wall	-

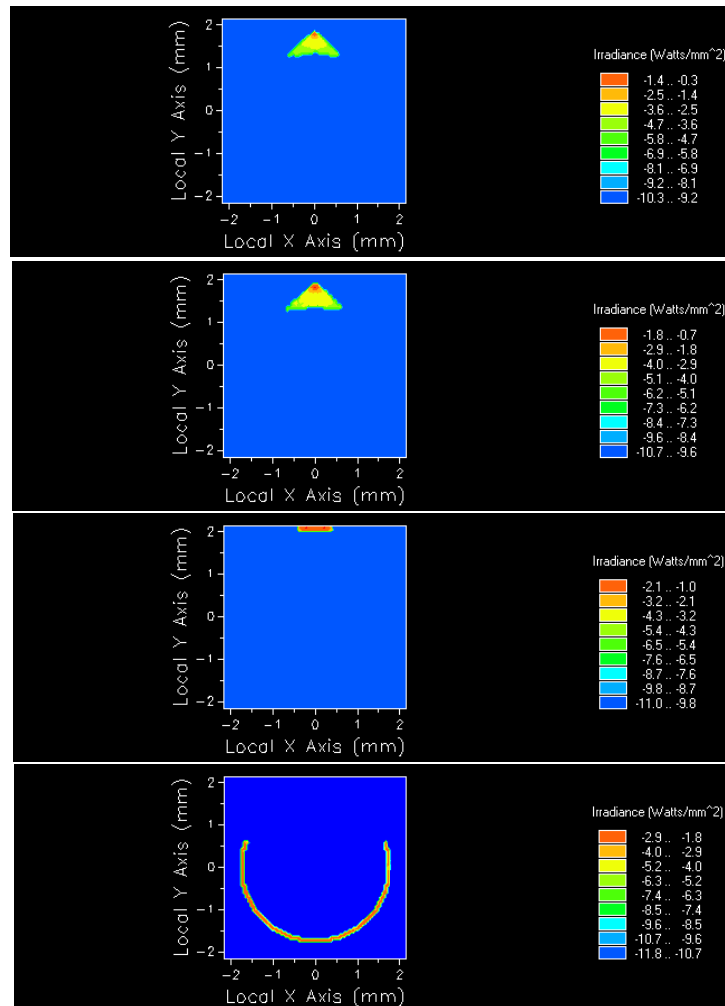Table 25. 15° Off-Axis Ghosts

Figure 48. 15° Off-Axis Ghost Images

OUT OF FIELD GHOSTS

The out of field ghost images were combined into one section. Here we see that all of these ghost images are caused by specular reflections off of mechanical structure within the barrel. The specific structures of interest are displayed in table 26 and can be visualized in figure 49. Notice how the reflections off the aperture maintain the circular structure.

AOI (°)	Ray Path	1st Ghost Surface	2nd Ghost Surface
20	26	Optical Space 2-B.Spline Surface 3	-
20	21	Optical Space 2-B.Spline Surface 22	-
20	84	Optical Space 3-B.Spline Surface 31/Detector	Lens 5 Bevel 2
25	13	Optical Space 1-B.Spline Surface 5	-
25	9	A.S. Inner Wall	Optical Space 4-B.Spline Surface 2
27	69	A.S. Inner Wall/Lens 2 Surface 2	Optical Space 3-B.Spline Surface 2
27	67	A.S. Inner Wall/Lens 2 Surface 2	Lens 1 Surface 2

Table 26. 20° Off-Axis Ghosts

To mitigate this issue, the mechanical design would have to be changed to appropriately baffle the system. The lens barrel design has three prominent sources for specular reflections:

- Lens barrel design
- Inner walls of apertures
- Planar surfaces

During the mechanical design of the lens barrel, the ray bundles represented by the FOV of the lens were used as guides to draw the lens barrel so that it would not vignette the beam. This method produced various conical shapes along the inside of the barrel which had surfaces that were parallel to the FOV ray bundle. As the source moved out of the field of view, the ray bundle approached a grazing incidence to these conical surfaces which allowed for specular reflections. From a radiometric standpoint, these conical structures are said to have subtend a larger projected solid angle from the point of view of the detector. By changing the lens barrel from a conical shape to a cylindrical shape the projected solid angle of lens barrel can be reduced thereby minimizing the stray light from this structure [33].

In addition, it was seen that the finite width of apertures served as specular reflection sources. Specifically, the inner wall of the aperture stop was the main source of reflection. Depending of the angle of incidence, light would either reflect off this surface and directly reach the detector or it would reflect off this surface then ghost again before reaching the detector. The only mitigation for this is to thin the inner wall of the aperture such that it subtends less of a projected solid angle from the point of view of the source i.e. make it more like a knife edge.

The last technique possible to improve the ghost images is a technique known as lens bending. Lens bending is a method used to mitigate the in focus/high irradiance images seen on the detector plane caused by planar surfaces [32]. While some planar surface such as windows and filters cannot be altered to improve performance other surfaces like lens surfaces can be. The goal of lens bending is to minimize the amount of planar surfaces within an optical system. These planar surfaces act like a cavity and easily enable reflections between them. Lens bending can be performed in a lens design software

such as ZEMAX where a merit function can determine the appropriate lens curvatures to minimize ghosts.
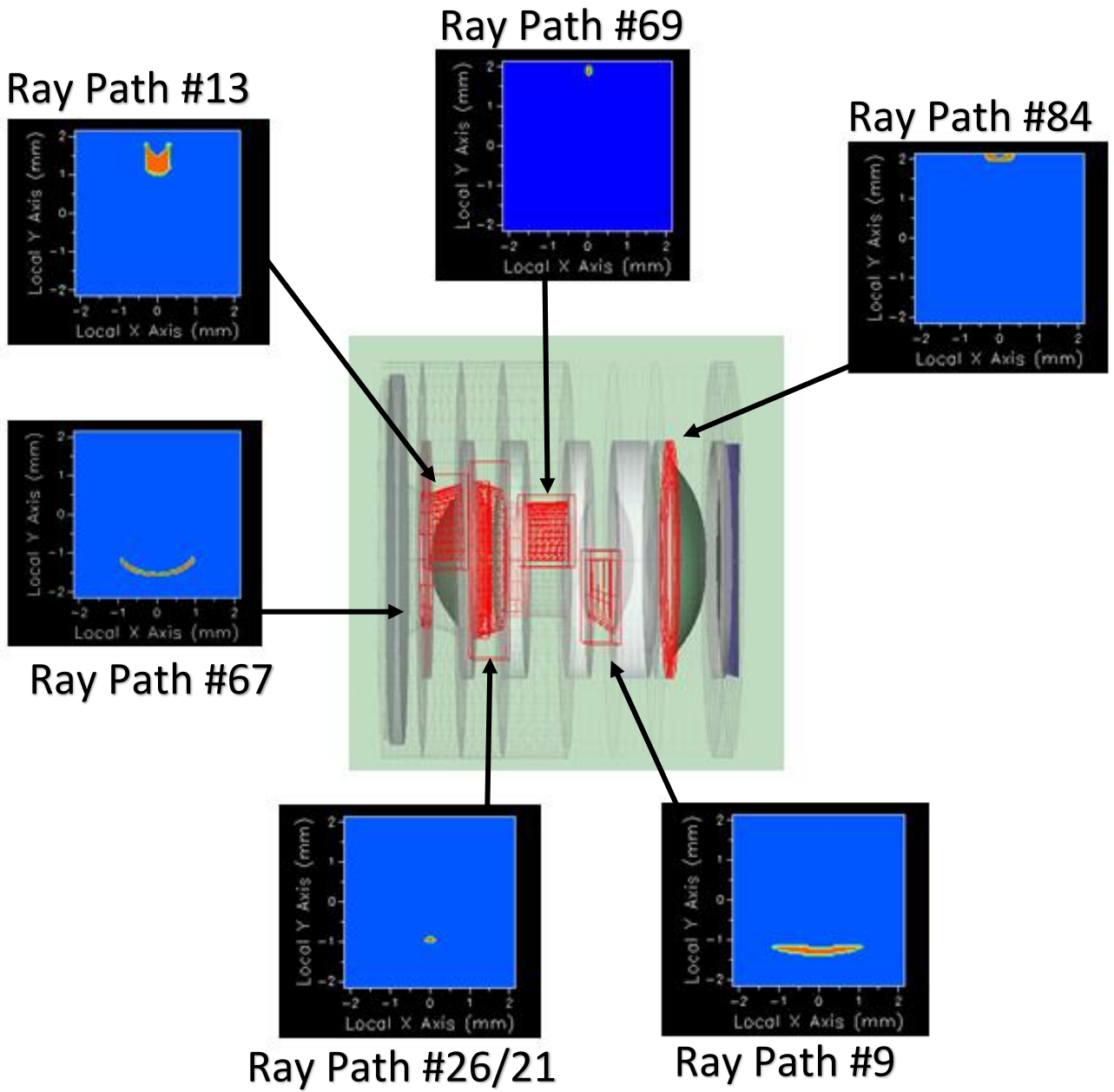

Figure 49. 20° Off-Axis Ghost Images

SCATTER ANALYSIS

The scatter analysis of the iPhone6 camera system considers only first-level scatter paths. The source used was the same source for the ghost image analysis. The raytrace controls were set to "allow all" for every common object. Allow all implies that the ray can either be a specular transmitted ray, a specular reflected ray, a specular total internally reflected ray, a scattered reflected ray or a scattered transmitted ray. The scatter analysis was performed using the point source transmittance (PST) method. As described in the name, the PST analyzes the transmittance of a point source through an optical system as a measurement of the ratio of the total irradiance reaching the detector to the total irradiance incident, as shown in equation 15.

$$PST(\theta, \phi) = \frac{E_{det}(\theta, \phi)}{E_{inc}(\theta, \phi)} = \frac{E_{det}(\theta, \phi)}{P_{\perp inc} * \cos(\theta)/A_{EP}} \tag{15}$$

The PST analysis examined both in-field and out-of-field stray light contributions by varying the angle of incidence from 0° to 80° in steps of 2°. That being said, the energy on the detector is a contribution of multiple stray light sources. However, this section will ignore any ghost reflections at grazing incidence because those ghost paths were examined in the previous section. Once the PST calculation was performed, the path details can be examined to determine if they are first-level scatter paths. If so, then a mitigation strategy can be assigned. To automate the PST calculation, a script was written in FRED and produced the following plot. The script is attached in the appendix.
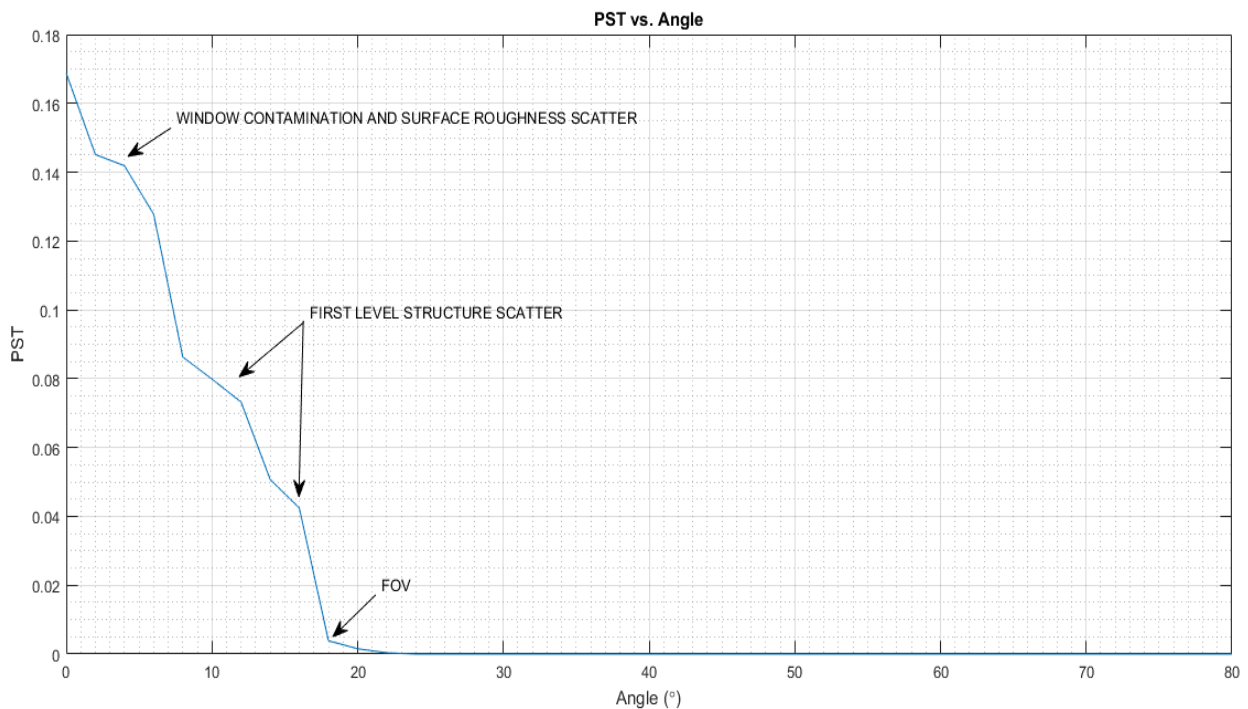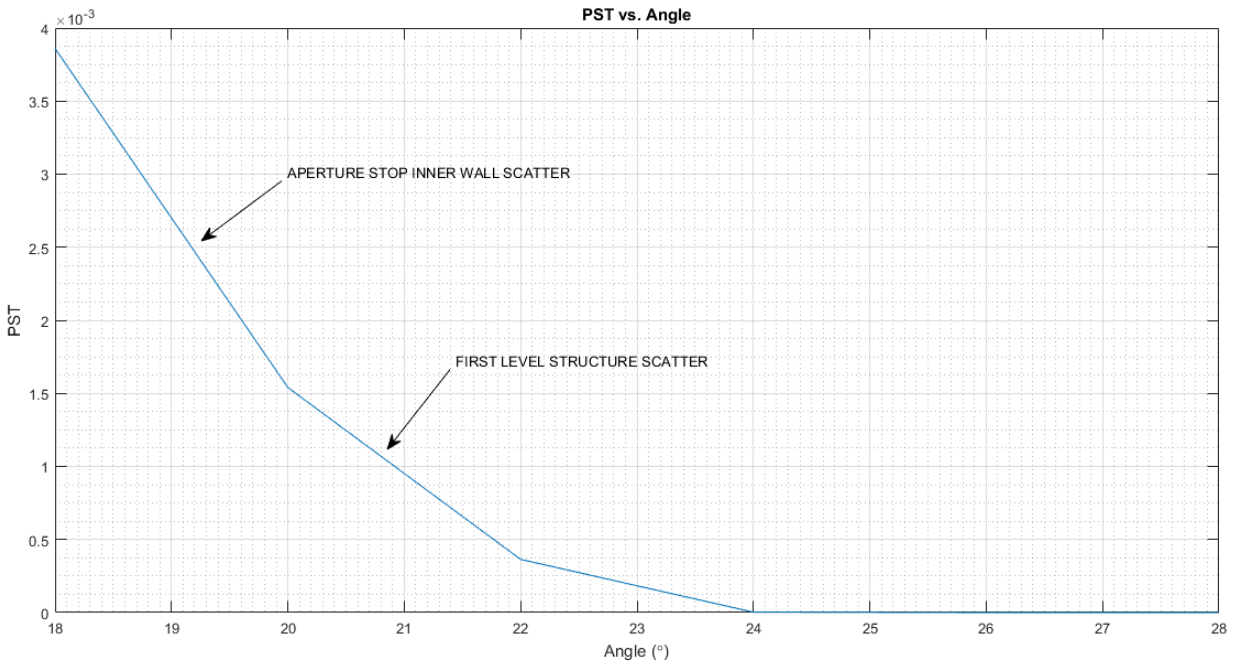

Figure 50. Full Field PST

Figure 51. Out-of-Field PST

Note that the in-FOV PST experiences a drop off--this is not ideal. Ideally, the PST should remain constant over the FOV but it will be shown that some of the barrel design choices were poor and partially obstructed the FOV thus causing the in-FOV PST to drop.

In a well baffled system, the PST plot will decay smoothly. Any abrupt, piecewise-like breaks in the PST curve or increase in the slope signifies a change in the scatter events. For the purpose of this exercise, I investigated the ray paths which exhibited these criteria. Additionally, all ray paths outside the field of view were investigated because outside the FOV only scattered light will reach the detector. Table 27 contains the top four scatter events for each source angle that was investigated.

AOI (°)	Ray Path	# Rays	Power (%)	Scatter Power (W)	1st Scatter Surface
4	3	956	0.2042	0.00512	Outer Window Surface 1
4	10	1173	0.0965	0.00242	Outer Window Surface 2
4	18	1164	0.0874	0.00219	Lens 2 Surface 2
4	22	1099	0.0844	0.00212	Lens 3 Surface 2
10	44	760	11.482	0.00236	Lens 5 Surface 2
10	11	772	9.739	0.00201	Outer Window Surface 2
10	3679	40	8.842	0.00182	Optical Space 4-B.Spline Surface 31
10	4	637	7.204	0.00149	Outer Window Surface 1
12	57	960	1.744	0.02390	Lens 5 Surface 2
12	3270	68	0.1760	0.00242	Optical Space 4-B.Spline Surface 31
12	47	511	0.1606	0.00220	Lens 4 Surface 2
12	4	796	0.1222	0.00167	Outer Window Surface 1
16	1785	536	14.054	0.001302	Optical Space 6-B.Spline Surface 22
16	64	1167	12.792	0.0011859	Lens 5 Surface 2
16	16	1374	10.235	0.0009488	Outer Window Surface 2
16	9	1122	10.06	0.0009326	Outer Window Surface 1
18	146522	48	4.206	0.0056828	Optical Space 3-B.Spline Surface 31
18	154	123	0.835	0.00112823	Lens 5 Bevel 2
18	9	1187	0.585	0.000790553	Outer Window Surface 1
18	459	1	0.513	0.000692561	Optical Space 5-B.Spline Surface 31
20	145	254	59.848	0.013140594	Optical Space 3-B.Spline Surface 31
20	25	35	1.997	0.00043848	Aperture Stop Inner Wall
20	13	1724	0.823	0.00018069	Outer Window Surface 1
20	188527	7	0.725	0.00015907	Optical Space 1-B.Spline Surface 5
22	143	563	53.13	0.01390192	Optical Space 3-B.Spline Surface 31
22	261	36	2.788	0.0007272073	Optical Space 2-B.Spline Surface 3
22	974	30	2.166	0.0005647669	Optical Space 2-B.Spline Surface 22
22	221	36	1.523	0.0003971551	Optical Space 1-B.Spline Surface 5
24	148654	106	54.318	0.0022667846	Optical Space 3-B.Spline Surface 31
24	295	35	16.968	0.0007081105	Optical Space 2-B.Spline Surface 22
24	150	56	15.33	0.0006397645	Optical Space 1-B.Spline Surface 5
24	39	23	3.1457	0.000131274	Aperture Stop Inner Wall

Table 27. First-Level Scatter Results

The scattered profiles were captured at the detector/image plane and produced the following plots in
log-base 10 space such that any low level detail could be visualized.
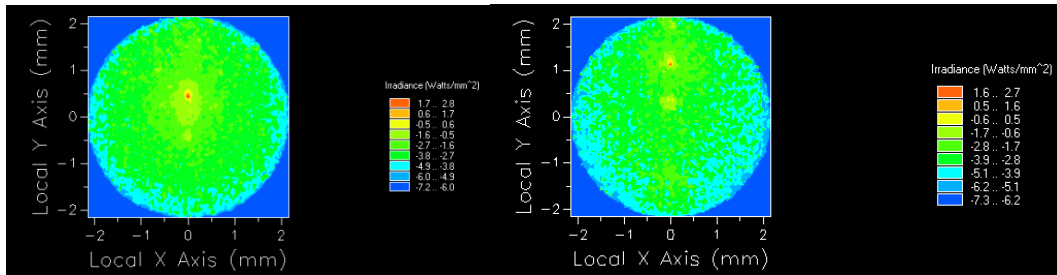
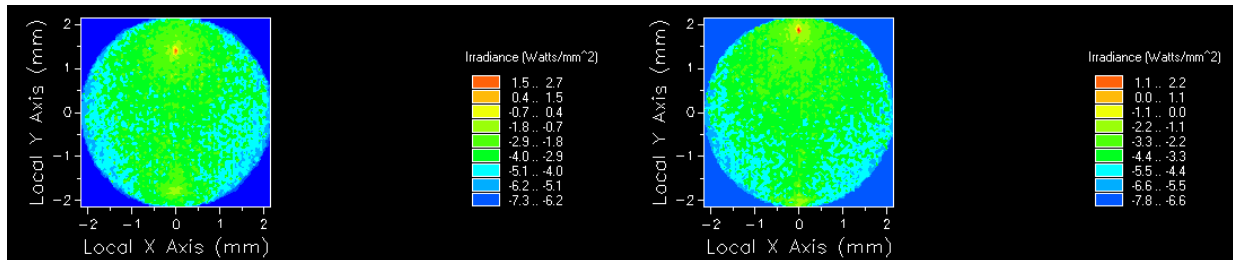Figure 52. 4° and 10° Off-Axis Scatter Profiles

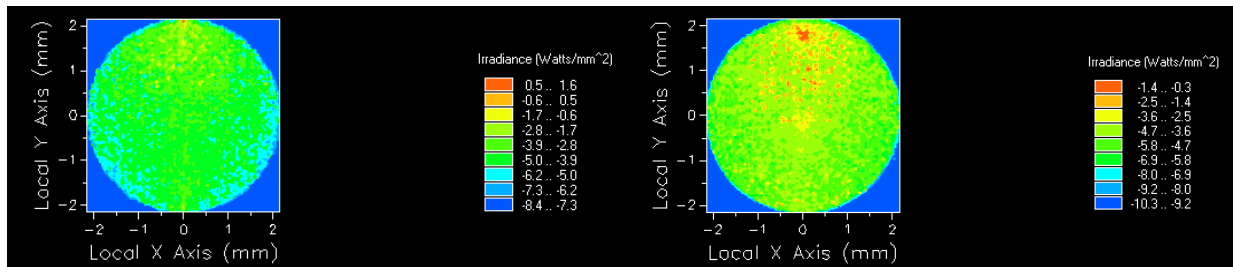Figure 53. 12° and 16° Off-Axis Scatter Profiles

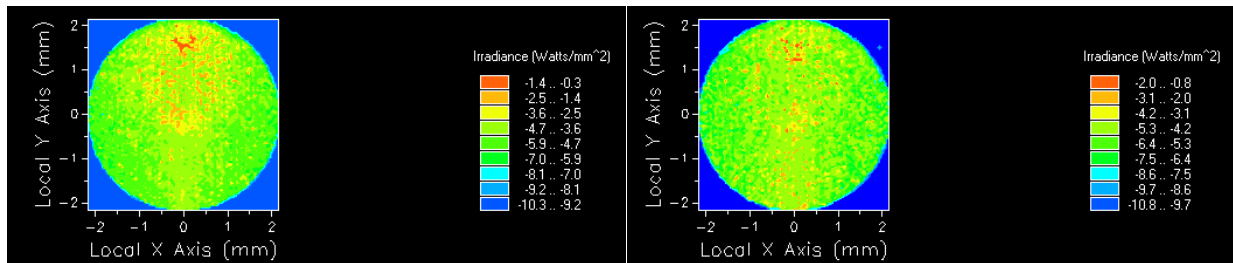Figure 54. 18° and 20° Off-Axis Scatter Profiles

Figure 55. 22° and 24° Off-Axis Scatter Profiles

Based on these findings it can be seen that particulate contamination on the window is the dominant form for scatter for source angles from four to ten degrees. Recall that the outer window was assigned a cleanliness value of 400, therefore, this is quite an easy problem to solve if the user keeps the window free of particulates. Surprisingly, this scatter event continues to be one of the top four dominant scatter sources all the way up to angle 20°. A particulate scatter event on the front surface of the window is shown in figure 56.
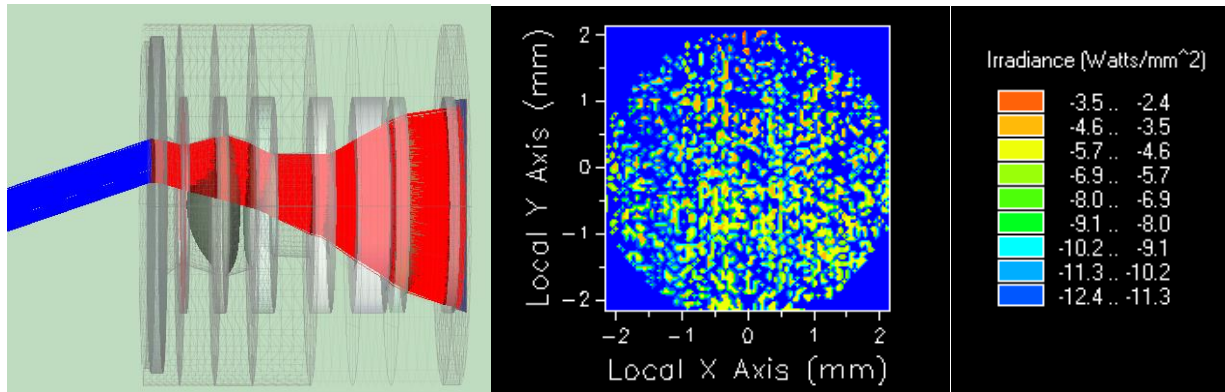
Figure 56. Window Scatter Event

As Pfisterer mentions, scatter will preserve the limiting resolution of the system but decrease image contrast [32]. It can be seen from the scatter profile in figure 56 that the particulate contamination on the outer surface of the window will cause a decrease in contrast over the entire detector because the extra energy will raise the SNR. Therefore, particulate contamination can be thought of as high-spatial frequency content when referencing table 16. Additionally, the polished lens surfaces will also cause wide-angle scatter and reduce the image contrast.

As the PST curves moves through ten degrees, the dominant scatter sources shift from particle contamination and polished lens surfaces to mechanical structure. With the exception of the outer surface of the window, all scatter outside the FOV is caused by mechanical structure. Of the out-of-field scatter, the dominant scatter sources are the inner walls of the aperture stop and the inner walls of the lens barrel for optical spaces 1 thru 6, as highlighted in figure 57.
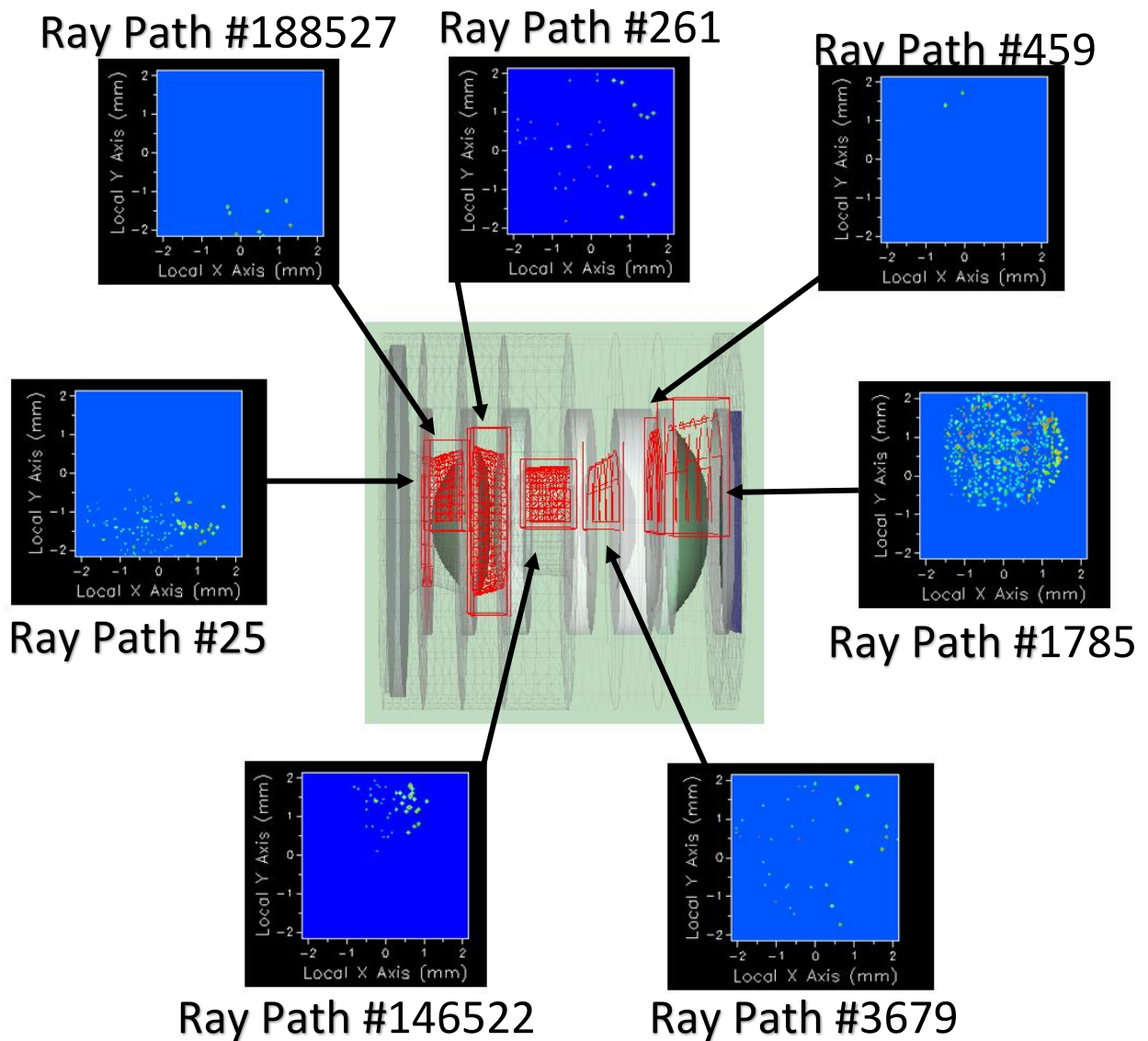
Figure 57. Barrel Scatter Sources

As mentioned in the ghost analysis section, to mitigate these scatter sources the design of the inner walls of the mechanical barrel will have to change from a conical shape to a cylindrical shape and the aperture wall will have to be thinned. The current material used for this lens barrel, PBT, has both specular and scatter characteristics. PBT is 7% reflective and has the same scatter properties as flat black paint, therefore, altering either of these properties will improve the stray light performance of the lens barrel.

X. CONCLUSIONS

The purpose of this project was not to solve the stray light issues of the iPhone 6 camera but rather to learn the foundations of stray light concepts, analysis and mitigation through the iPhone 6 camera system. As a prerequisite to stray light mitigation, both lens and opto-mechanic design are necessary skills. Although this paper did not explore any of the advanced lens or opto-mechanic design techniques used for mitigation, the ground-work presented allows for an easy transition into this exploration.

The results demonstrated that the implementation of common mitigation techniques can be performed to improve the stray light performance of the optical system. To improve the specular stray light performance of the system, such mitigation techniques as improving AR coatings of optics, lens bending and alternative lens barrel designs should be implemented. To improve the scattered stray light performance of the system, such mitigation techniques as surface roughening, material selection and alternative lens barrel designs should be explored. Notice that both mitigation groups demonstrate that a poor mechanical lens barrel design lead to a stray light issues. Although the design is not ideal, it did lead to some interesting results which were beneficial to the learning process. Once these mitigation strategies are implemented it is important to understand that it is an iterative process involving the lens and opto-mechanical design [18]. As Pfisterer mentions [34], the two most time consuming tasks for stray light project is the design of the mechanical model and the stray light calculations. For future work, more time should be spent researching and developing a mechanical design before the design process begins. In addition, it was discovered that particle contamination and polished lens surfaces acted as high-spatial frequency content which decreased the image contrast while maintaining the resolution for scatter stray light sources.

In addition to the design lessons learned, I also learned about the importance of having adequate hardware to ensure that the simulations could be performed in a timely manner. On the same note, for the purposes of data processing it is very useful to learn to FRED scripting tools. I was able to write a short script for my PST calculations but was lacking a working code for my RMS irradiance calculations. Improving my scripting skills will allow me to not only perform some of the basic calculations but save me a lot of time. I look forward to advancing my knowledge on stray light analysis and applying these lessons learned on future design applications.

References

[1] R. Pfisterer, Stray Light Short Course, October 25 ed., Tucson, AZ: Photon Engineering, 2015, p. 13.

[2] J. Sasian, "OPTI 517 Lecture 2: First Order Review," College of Optical Sciecnes, Tucson, 2015.

[3] E. Fest, "Stray Light Control for Molded Optics," in *Molded Optics: Design and Manufacture*, Boca Raton, FL: CRC Press, 2011, p. 119.

[4] S. Baumer, "Coating on Plastics," in *Handbook of Plastic Optics*, 2nd ed., Weinheim, Wiley-VCH Verlag GmbH & Co., 2010, p. 179.

[5] J.-T. Makinen, "Cost Modeling of Injection-Molded Plastic Optics," in *Handbook of Plastic Optics*, 2nd ed., Weinheim, Wiley-VCH Verlag GmbH & Co., 2010, p. 234.

[6] M. Pfeffer, "Optomechanics of Plastic Optical Compenents," in *Handbook of Plastic Optics*, 2nd ed., Weinheim, Wiley-VCH Verlag GmbH & Co., 2010, p. 9.

[7] R. Juergens, "Image Quality," Raytheon Missle Sysems, Tucson, 2015.

[8] R. Pfisterer, Stray Light Short Course, October 25 ed., Tucson, AZ: Photon Engineering, 2015, p. 59.

[9] R. Pfisterer, Stray Light Short Course, October 25 ed., Tucson, AZ: Photon Engineering, 2015, pp. 294-95.

[10] R. I. Mercado, "Small Form Factor Telephoto Camera". USA Patent 9,223,118 B2, 29 December 2015.

[11] K. Minami, "Optical Plastics," in *Handbook of Plastic Optics*, 2nd ed., Weinheim, Wiley-VCH Verlag GmbH & Co., 2010, p. 127.

[12] J. Sasian, "OPTI 518 Lecture 12 Notes," College of Optical Sciences, Tucson, 2016.

[13] J. Sasian, "OPTI 517 Lecture 11 Notes," College of Optical Sciences, Tucson, 2015.

[14] E. Fest, "Stray Light Control for Molded Optics," in *Molded Optics: Design and Manufacture*, Tucson, AZ: CRC Press, 2011, p. 84.

[15] I. ThorLabs, 2 May 2016. [Online]. Available: http://www.thorlabs.us/newgrouppage9.cfm?objectgroup_id=3279.

[16] U. Schulz, "Coating on Plastics," in *Handbook of Plastic Optics*, 2nd ed., Weinheim, Wiley-VCH Verlag GmbH & Co., 2010, p. 181.

[17] Adimec, 3 May 2016. [Online]. Available: http://info.adimec.com/blogposts/bid/40330/Anti-reflection-coatings-improve-accuracy-for-high-performance-cameras.

[18] E. Fest, "Stray Light Control for Molded Optics," in *Molded Optics: Design and Manufacture*, Boca Raton, FL: CRC Press, 2011, p. 96.

[19] "Institute of Environmental Sciences and Technology," LEST, [Online]. Available: www.lest.org. [Accessed 10 05 2016].

[20] R. Pfisterer, Stray Light Short Course, Tucson, AZ: Photon Engineering, 2015, p. 200.

[21] P. F. M. &. L. A. Ma, "Surface Particle Obscuration and BRDF Predictions," *Proceedings SPIE,* vol. 1165, p. 199, 1989.

[22] J. Lindberg and J. Gillespie, "Relationship between particle size and imaginary index is atmospheric dust," *Applied Optics,* vol. 16, no. 10, 1977.

[23] R. Pfisterer, Stray Light Short Course, Tucson, AZ: Photon Engineering, 2015, p. 252.

[24] R. Pfisterer, Stray Light Short Course, Tucson , AZ: Photon Engineering, 2015, p. 256.

[25] H. H. Barrett, "Psychophysics, Model Observers and Image Quality," Tucson, 2016.

[26] J. Harvey, "Light Scattering Characteristics of Optical Surfaces (Ph.D. dissertation)," University of Arizona, Tucson, 1976.

[27] J. &. L. K. Harvey, "Scattering from Multilater Coatings: A Linear Systems Model," *Proceedings SPIE,* vol. 1530, 1991.

[28] J. &. K. A. Harvey, "Scattering Effects from Residual Optical Fabrication Errors," vol. 2576, pp. 155-174, 1995.

[29] R. Pfisterer, Stray Light Short Course, Tucson, AZ: Photon Engineering, 2015, p. 622.

[30] J. &. M. L. Bennett, "Introduction to Surface Roughness and Scattering," *Optical Society of America,* p. 92.

[31] R. Pfisterer, Stray Light Short Course, Tucson, AZ: Photon Engineering, 2015, pp. 366-369.

[32] R. Pfisterer, Stray Light Short Course, Tucson, AZ: Photon Engineering, 2015, pp. 609-626.

[33] R. Pfisterer, Stray Light Short Course, Tucson, AZ: Photon Engineering, 2015, pp. 574-576.

[34] R. Pfisterer, Stray Light Short Course, Tucson, AZ: Photon Engineering, 2015, p. 297.

[35] R. Pfisterer, Stray Light Short Course, October 25 ed., Tucson, AZ: Photon Engineering, 2015, p. 18.

[36] R. Pfisterer, Stray Light Short Course, Octobe 25 ed., Tucson, AZ: Photon Engineering, 2015, p. 98.

[37] M. Pfeffer, "Optomechanics of Plastic Optical Components," in *Handbook of Plastic Optics*, 2nd ed., Weinheim, 2010, p. 16.

[38] M. Pfeffer, "Optomechanics of Plastic Optical Components," in *Handbook of Plastic Optics*, 2nd ed., Weinheim, Wiley-VCH Verlag GmbH & Co., 2010, pp. 15-16.

APPENDIX: PST SCRIPT

```vb
'PST Calculation
Dim op As T_OPERATION, pRay As T_RAY, PST As Double
Dim detArea As Double
Dim angle As Double
Dim node As Long
Dim detNode As Long
Dim adv As T_ADVANCEDRAYTRACE
Dim semiWidthX As Double, semiWidthY As Double
Dim num As Long
Dim isEllipse As Boolean
Sub Main

    node = Find
    FullName( "Optical Sources.PST Source" )
    Print "found PST source at node " & node
    detNode = FindFullName( "Geometry.Image Plane.Surf 21" )
    Print "Found detector at node " & detNode

    detArea = 4.367886545^2 'in mm for detector
    EnableTextPrinting(False)

    For angle = 0 To 80 Step 2

        SetSourceDirection node, 0, Tan( angle * 0.017453 ), 1
success = GetSourcePosGridRandom ( node, semiWidthX, semiWidthY, num,
isEllipse )
        If angle < 10 Then
            num = 100
        ElseIf angle > 10 And angle < 20 Then
            num = 500
        ElseIf angle > 20 And angle < 30 Then
            num = 1000
        ElseIf angle > 30 And angle < 40 Then
            num = 100000
        Else
            num = 1000000
        End If
        SetSourcePosGridRandom node, semiWidthX, semiWidthY, num, isEllipse
        Update
        DeleteRays
        InitAdvancedRaytrace adv
        adv.draw = False
        adv.rayPaths = True
        adv.rayHistory = True
        count = AdvancedRaytrace( adv)

        PST = GetSurfIncidentPower(detNode) * Cos( angle * 0.017453 )/detArea

        EnableTextPrinting(True)
        Print "PST at " & angle & " degrees = ";Chr(9);Chr(9);PST
        EnableTextPrinting(False)

    Next angle
    EnableTextPrinting(True)
End Sub
```